4
Extension and Torsion

The deformations experienced by some biological tissues and biomaterials can be very complex. For example, we have seen that all six components of the Green strain [cf. Eq. (2.42), but relative to cylindrical coordinates] are nonzero in the wall of the heart, and each varies with position and time throughout the cardiac cycle (cf. Fig. 2.20). In such cases, we must often resort to sophisticated numerical methods to measure or compute the strain fields. Nevertheless, there are many cases in which the deformations are much simpler, as, for example, in chordae tendineae within the heart, which experience primarily an axial extension with associated lateral thinning (cf. Fig. 3.2). Indeed, as an introduction to biomechanics, it is often best to study simple motions such as extension, compression, distension, twisting, or bending, which allow us to increase our understanding of the basic approaches and which also apply to many problems of basic science or clinical and industrial importance. Whereas we considered small strains that occur during a simple inflation of a thick-walled tube in the last section of Chap. 3, here we consider in some detail small strains associated with axial extension and torsion, with an associated complete stress analysis for the latter for a linear, elastic, homogenous, and isotropic (LEHI) behavior of a circular member. Such analyses will be particularly relevant in bone mechanics.

Observation 4.1. The reader is encouraged to consult Carter and Beaupré (2001) for a description of the mechanobiology of skeletal *development*. Here, we simply recount some of their observations. For example, they write: "The flat bones of the skull and face are formed by intramembranous ossification within a condensation of cells derived from the neural crest. In the limb bones and most of the postcranial skeleton, however, mesenchymal cell condensations chondrify, creating the endoskeletal cartilage anlagen. These cartilage

J.D. Humphrey, S.L. O'Rourke, *An Introduction to Biomechanics*,
DOI 10.1007/978-1-4939-2623-7_4

rudiments form the templates for the future skeleton and subsequently, in the process of growth, undergo a bony transformation." In particular, "The cartilage cells within the rudiments therefore undergo a characteristic process of cell proliferation, maturation, hypertrophy, and death, followed by matrix calcification and ossification. Variations within the cartilage growth and ossification rates in different directions within the anlage result in shape changes of developing bones . . . Once a region of cartilage mineralizes and it is either resorbed or replaced by bone, further bone growth occurs by osteoblastic apposition on mineralized surfaces." As noted in Chap. 12, Developmental Biomechanics is one of the exciting frontiers of our field, one that is clearly complex.

Many factors affect the development as well as the subsequent maintenance and adaptation of bone. For example, biological factors that affect the metabolism of chondrocytes include bone-derived growth factor (BDGF), bone morphogenetic proteins (BMP), cartilage-derived morphogenetic protein (CDMP), fibroblast growth factors (FGFs), insulin-like growth factors (IGFs), interleukins (ILs), sex hormones, prostaglandins, matrix metalloproteinases (MMPs) and their inhibitors (TIMPs), and even vitamins A, C, and D. In addition, of course, mechanical stimuli also play a major role in the development, maintenance, and adaptation of bone. In many cases, strains have proven convenient to correlate with the mechanotransduction. Let us now consider measures of the deformation in the simple case of axial loading.

4.1 Deformations Due to Extension

4.1.1 Biological Motivation

Figure 4.1 illustrates some of the important structural and biological features of a representative mature long bone. Grossly, the three primary regions are the central long hollow shaft, the end caps, and the transitional regions between the two. These three regions are referred to respectively as the diaphysial, epiphysial, and metaphysial regions. The central core of the diaphysial region is called the medullary canal; it contains the bone marrow, which produces different types of blood cells and their precursors. Of primary concern here, however, is that there are two primary classes of bone tissue: *cortical* (or compact) and *cancellous* (or trabecular). Cortical bone constitutes most of the outer portion of a whole bone, including the majority of the wall of the diaphysis. Except in a few regions, the cortical bone is invested by a specialized covering, the periosteum, which is rich in collagen and fibroblasts and has an underlying osteogenic layer that contains active bone cells. During development and in periods of trauma and repair, cortical and cancellous bone can be of the woven type, which is often poorly structured, highly mineralized, and appears to serve as a temporary scaffolding for the development of another type of bone tissue.

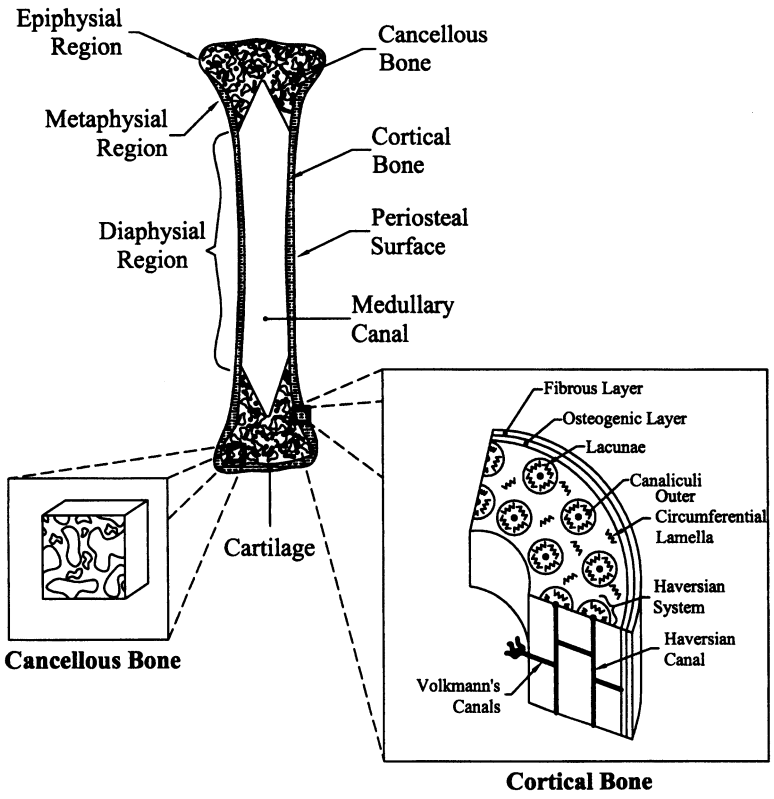

FIGURE 4.1 Schema of the structure of a typical long bone, which consists of the diaphysial (shaft) region, the metaphysial (transition) region, and the epiphysial (end) regions. Note, too, the two primary types of bone tissue: cortical, which is found along the outer surface, and cancellous, which is found in the inner portion of the end regions. The cartilage forms as a protective covering at the end of the articulating bones; cartilage is discussed in Chap. 11.

In maturity and following healing, cortical bone consists primarily of two types of bone: *Lamellar* bone is characterized by concentrically arranged layers (or laminae), each about 20 μm thick, with networks of blood vessels between layers; *osteonal*, or Haversian, bone is characterized by nearly cylindrical units (or osteons) ~200 μm in diameter and ~2 cm long, which contain centrally located blood vessels connected to radial channels called Volksmann's channels. Each of these channels, which allow the transport of blood and bone fluid within compact bone, contribute to an overall porosity despite the otherwise dense constitution of cortical bone (specific gravity ~2). Uniformly distributed throughout the interstitial substance of cortical bone are lenticular cavities, called lacunae, each containing a bone cell called an osteocyte. Radiating in all directions from each lacunae are anastomosing tubular passages, called canaliculi, which further contribute to the porosity and are essential to nutrient exchange.

Cancellous bone has a very different microstructure. It is much more porous, consisting of a three-dimensional lattice of branching trabeculae, which are thin-walled and of lamellar type. Cancellous bone is found, for example, near the ends of long bones. Recall from Chap. 1 that research in the late nineteenth century by von Meyer, Culmann, and Wolff suggested that the orientation of the trabeculae in the femur appeared to follow the directions of the principal stresses (Fig. 4.2). This ultimately led to "Wolff's law of bone remodeling,"

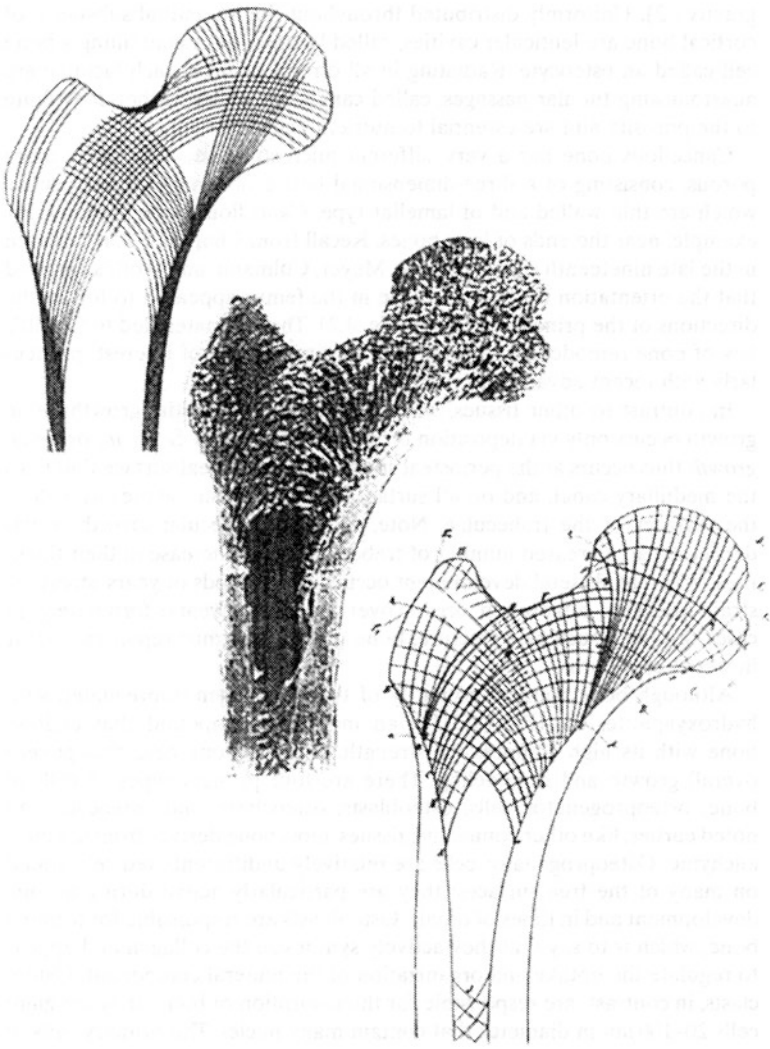

FIGURE 4.2 Correspondence between the trabecular structure in the femur and Wolff's envisioned lines of tension. [From Wolff (1986), with permission from Springer].

a topic that continues to be of interest, particularly with recent advances in mechanobiology.

In contrast to other tissues, which experience interstitial growth, bone growth occurs only via deposition on cell-laden surfaces. Such *appositional growth* thus occurs at the periosteal surface, the endosteal surface that lines the medullary canal, and on all surfaces of the tubular cavities as well as the surfaces of the trabeculae. Note, too, that trabecular growth is evidenced by an increased number of trabeculae or an increase in their thickness. Whereas skeletal development occurs over periods of years, stress- or strain-mediated adaptation occurs over months to years; fortunately, in cases of injury, such as a fracture, bone growth and thus repair can occur in weeks to months.

Although bone consists primarily of type I collagen impregnated with hydroxyapatite, $Ca_{10}(PO_4)_6(OH)_2$, an inorganic compound that endows bone with its high compressive strength, it is the bone cells that govern overall growth and remodeling. There are four primary types of cells in bone: osteoprogenitor cells, osteoblasts, osteoclasts, and osteocytes. As noted earlier, like other connective tissues, most bone derives from the mesenchyme. Osteoprogenitor cells are relatively undifferentiated cells found on many of the free surfaces; they are particularly active during normal development and in times of repair. Osteoblasts are responsible for forming bone, which is to say that they actively synthesize the collagen and appear to regulate the uptake and organization of the mineral component. Osteoclasts, in contrast, are responsible for the resorption of bone; they are giant cells 20–100 μm in diameter that contain many nuclei. The primary cells of fully formed bone are the osteocytes, which derive from the osteoblasts and reside in the lacunae within the interstitial space (Fig. 4.3). Once encased in calcified bone matrix, the osteocytes no longer divide; rather, they form gap junctions with neighboring osteocytes via the canaliculi, and probably participate in the control of the osteoblasts and osteoclasts. For more on the biology of bone, see Alberts et al. (2008) and Fawcett (1986).

One of the key questions in bone mechanobiology is how the embedded osteocytes or surface osteoblasts/osteoclasts sense and respond to changes in mechanical stimuli. We know, for example, that there is tremendous bone loss in load-bearing bones (particularly in the legs) in bedridden patients and astronauts in a microgravity environment. Conversely, there is significant increase in bone mass in athletes such as weight lifters and even tennis players (e.g., the humerus can have a 30 % greater cross-sectional area in the playing versus the nonplaying arm). Such examples of decreased and increased bone mass are likewise common when applied loads are altered clinically, such as due to bone screws, plates, or implanted prostheses. For more examples, see Carter and Beaupré (2001). It is not clear, however, if the causative cellular activity correlates best with changes in stress, strain, strain rate, strain energy, or similar metric. Again, we emphasize that cells cannot directly sense these

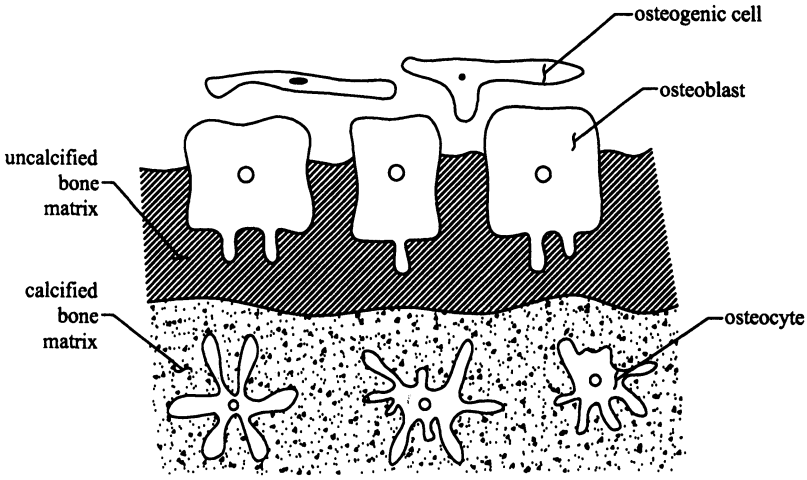

FIGURE 4.3 Schema of three of the four primary bone cells. The osteogenic cell, the osteoblast (or bone-forming cell), and the osteocytes, which are former osteoblasts that are trapped within calcified bone matrix. Not shown are the osteoclasts, which remove bone tissue.

volume-averaged continuum quantities, yet they will likely be very useful for identifying such empirical correlations (Humphrey 2001). Although strains can be measured on the outer surface of some bones, it is not possible to measure internal strains or any stresses. Hence, we must resort to the methods of mechanics to calculate the stress or strain fields experienced by the bone of interest, which, in turn, requires knowledge of the geometry, material properties, and applied loads. As noted in Chap. 2, bones can be described by Hooke's law for stress analysis in many circumstances, yet a detailed study of the mechanobiology may require structural models that account for the fine trabecular architecture or material models that account for the porosity and, indeed, the internal flow of blood or bone fluid due to applied loads. The latter necessitates modeling of the solid–fluid coupling, which is addressed briefly in Chap. 11 in a different context. Solid–fluid coupling in bone is an advanced topic of current research. Here, therefore, let us consider the simplest approach, assuming on average that bone exhibits a linear, elastic, locally homogenous, and isotropic (i.e., LEHI) behavior under some circumstances. In this case, effective bone properties can be assumed to be $E \sim 15$ GPa and $\nu \sim 0.33$. Indeed, let us consider the stress and strain fields in the diaphysial region of a long bone, consisting of cortical bone only and subject, first, to an axial compressive load and, second, to a twisting moment as suggested by Fig. 4.4; of course, the bone could also experience bending loads, but these are considered in Chap. 5.

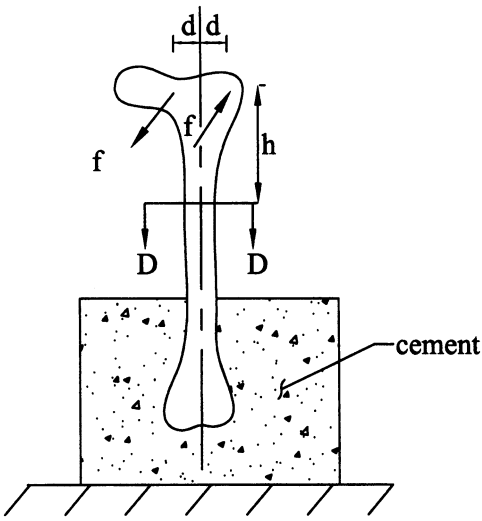

FIGURE 4.4 Schema of a portion of the femur isolated in the laboratory for mechanical testing to induce torsion via the application of a couple $2fd$.

4.1.2 Theoretical Framework

Envision a case in which a rod of negligible weight is suspended vertically from a fixed support and loaded from the lower end by a constant force that is applied through its centroid and uniformly over the cross-sectional area. Intuitively, the axial displacement (say, u_x) will be zero at the fixed support, nonzero in the middle, and maximum at the lower end (Fig. 2.18); that is, the displacement will vary along the length of the rod (even though the stress is assumed to be constant throughout), from which we can compute the axial strain, namely

$$u_x = u_x(x) \rightarrow \varepsilon_{xx} = \frac{\partial u_x}{\partial x}. \tag{4.1}$$

Reminder: This formula for strain is restricted to small values, consistent with our desired use of Hooke's law as a descriptor of LEHI behavior. Clearly, integration of ε_{xx} with respect to x can provide the displacement at any point x, including that at the lower end $x = L$; that is,

$$\int_0^x \varepsilon_{xx} dx \equiv \int_0^x \frac{\partial u_x}{\partial x} dx = u_x(x) - u_x(0), \tag{4.2}$$

where $u_x(0) = 0$ is the displacement boundary condition (for this case) at the fixed end. Now, ε_{xx} can be related to the stress via Hooke's law [Eq. (2.69)],

where the uniform 1-D state of stress in an axially loaded rod is $\sigma_{xx} = f/A$ from Eq. (3.29). Hence, we have

$$\varepsilon_{xx} = \frac{1}{E}[\sigma_{xx} - \nu(0+0)] = \frac{f}{AE} \rightarrow u_x(x) = \int_0^x \frac{f}{AE}\, dx, \tag{4.3}$$

where, in general, the force, cross-sectional area, and even Young's modulus could vary with x. In the special case in which all three quantities are independent of x and we seek only the value of u_x at the lower end (the so-called end deflection δ), we have the simple result

$$u_x(x = L) \equiv \delta = \frac{fL}{AE}. \tag{4.4}$$

In general, however, it is best to remember the primary result of Eq. (4.3), which determines a *deformation in terms of the applied loads*, *geometry*, *and material properties*. It can be written generally as

$$u_x(x = c) - u_x(x = a) = \int_a^c \frac{f(x)}{A(x)E(x)} dx, \tag{4.5}$$

which emphasizes that the applied axial force, cross-sectional area, and Young's modulus may each vary with x. Of course, the integral is a linear operator and, thus,

$$\int_a^c \frac{f(x)}{A(x)E(x)} dx = \int_a^b \frac{f(x)}{A(x)E(x)} dx + \int_b^c \frac{f(x)}{A(x)E(x)} dx \tag{4.6}$$

and so forth. This division of the integral over separate domains can be very helpful in cases in which $f(x)$, $A(x)$, or $E(x)$ are constant over such subdomains. Let us illustrate via a few examples how this might be useful. First, however, note some terminology: If a rod is homogeneous, then $E \neq E(x)$; if a rod has a constant cross section, then $A \neq A(x)$; and if the rod is under a constant load, then $f \neq f(x)$.

Example 4.1 Consider a vertically mounted, axially loaded member subject to its own distributed weight w N/m (see Fig. 4.5a). Assume that the member has a constant cross-sectional area A and a constant elastic modulus E. The total weight of the member of length L is thus $W = wL$. Find the displacement u_x at the free end [i.e., $\delta \equiv u_x\ (x = L)$].

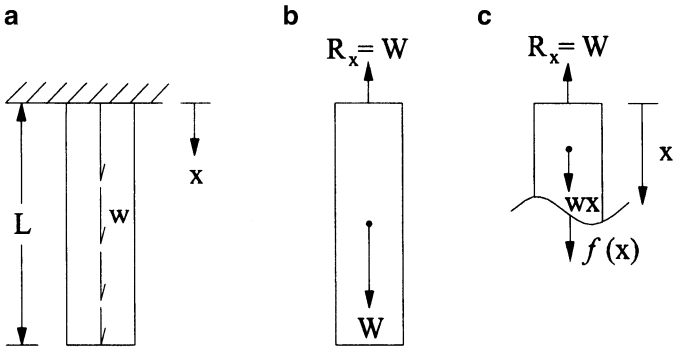

FIGURE 4.5 A vertically loaded member subject to its own weight, given as w (force per unit length) and thus a total weight $W = wL$, which acts at the center of gravity. Shown is the physical problem, a free-body diagram of the whole to isolate reaction R_x at the fixed support, and a free-body diagram of a part to isolate the internal force $f(x)$.

Solution: First, let us construct a free-body diagram of the whole structure and ensure equilibrium to find the reactions (Fig. 4.5b):

$$\sum F_x = 0,\ -R_x + W = 0 \rightarrow R_x = W = wL,$$
$$\sum F_y = 0,\ R_y = 0,$$
$$\sum M_z = 0,\ M_{wall} = 0.$$

Next, construct a free-body diagram of the parts (Fig. 4.5c) recalling that if a structure is in equilibrium, then each of its parts is in equilibrium. The force $f(x)$ due to the weight of the member is $w(L - x)$ at any cross section cut at a distance x from the support; at $x = 0$, $f(0) = R_x = wL$, the entire weight, as it should. Alternatively, in terms of the total weight of the member, the force becomes $W(1 - x/L)$ and thus

$$\sum F_x = 0 \rightarrow \int \sigma_{xx} dA - f = 0 \rightarrow \sigma_{xx} = \frac{f}{A} = \frac{W}{A}(1 - x/L).$$

Note that the stress is largest at $x = 0$, where all of the weight must be borne by the material, and the stress is zero at the free end, which is free of applied loads (i.e., traction-free). Given the stress, the strain and the axial displacement can now be computed using Hooke's law and Eq. (4.5); namely

$$\varepsilon_{xx} = \frac{1}{E}\left[\sigma_{xx} - \nu\left(\sigma_{yy} + \sigma_{zz}\right)\right]$$

with σ_{yy} and σ_{zz} each zero. Thus,

$$\varepsilon_{xx} = \frac{\sigma_{xx}}{E} \rightarrow \int_0^L \varepsilon_{xx} dx = u_x(x = L) - u_x(x = 0) = \int_0^L \frac{W(1 - x/L)}{AE} dx,$$

where $u_x = 0$ at $x = 0$ (a displacement boundary condition) and the end displacement is

$$\delta \equiv u_x(x = L) = \frac{W}{AE}\left(x - \frac{x^2}{2L}\Big|_0^L\right) = \frac{WL}{2AE}.$$

Of course, the displacement at any value of x is found by integrating from 0 to x rather than from 0 to L.

Example 4.2 Find the end displacement δ in each of the members illustrated in Fig. 4.6.

Solution: The first structure (Fig. 4.6a) is homogenous and subject to a constant axial load P, but it does not have a constant cross-sectional area. The area changes abruptly from A_1 to A_2 at $x = L/2$. Thus, $A = A(x)$ and the end displacement is determined via

$$u_x(x) - u_x(0) = \int_0^x \frac{P}{A(x)E} dx \rightarrow \delta = u_x(0) + \frac{P}{E}\int_0^L \frac{dx}{A(x)}.$$

The integral must be separated at the point of discontinuity in the cross-sectional area to give the following results [with $u_x(0) = 0$ via a boundary condition]:

$$\delta = \frac{P}{E}\int_0^{L/2} \frac{dx}{A_1} + \frac{P}{E}\int_{L/2}^L \frac{dx}{A_2} \rightarrow \delta = \frac{P}{A_1 E}\int_0^{L/2} dx + \frac{P}{A_2 E}\int_{L/2}^L dx,$$

or

$$\delta = \frac{PL}{2A_1 E} + \frac{PL}{2A_2 E} = \frac{PL}{2E}\left(\frac{1}{A_1} + \frac{1}{A_2}\right).$$

The second structure (Fig. 4.6b) has a constant cross-sectional area and is subjected to a constant axial load P, but it is not homogenous. The material

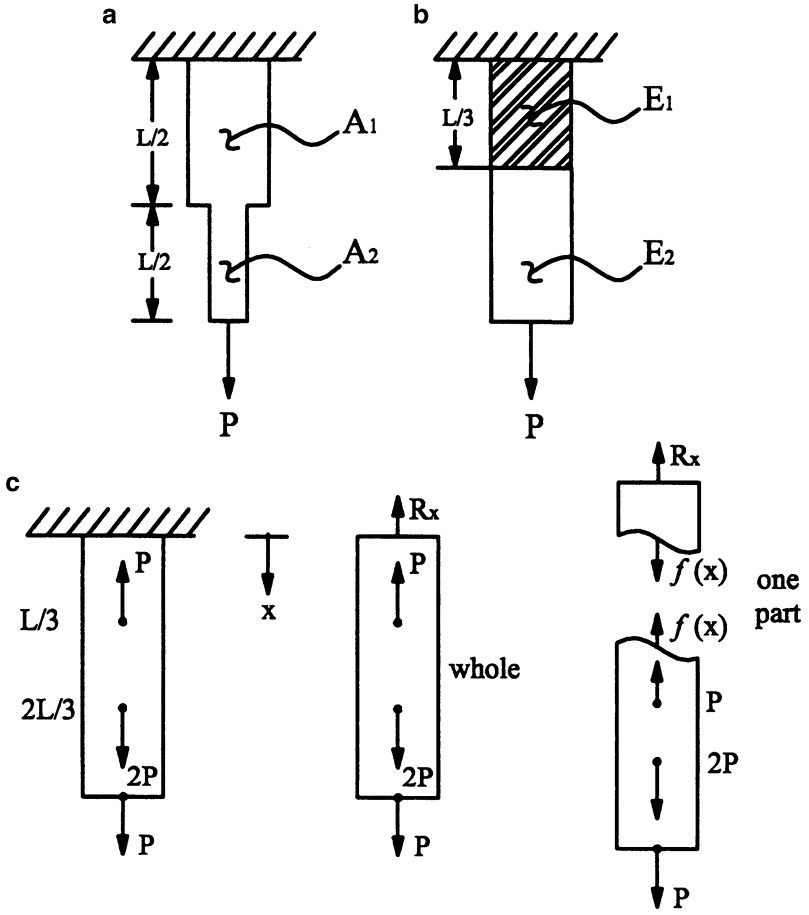

FIGURE 4.6 Axially loaded rods having a nonconstant cross section (panel **a**), a nonconstant material composition (panel **b**), and multiple applied loads (panel **c**). Although we need to draw free-body diagrams of the whole and multiple parts for each case, we show only the free-body diagram of the whole structure and one free-body diagram for a part of the rod of panel **c**.

properties change at $x = L/3$ from the wall. Therefore, $E = E(x)$ and the displacement becomes

$$u_x(x) - u_x(0) = \frac{P}{A}\int_0^x \frac{dx}{E(x)} \rightarrow \delta = u_x(0) + \frac{P}{A}\int_0^L \frac{dx}{E(x)}.$$

Again dividing the integration over judicious domains, we have

$$\delta = \frac{P}{A}\int_0^{L/3} \frac{dx}{E_1} + \frac{P}{A}\int_{L/3}^{L} \frac{dx}{E_2},$$

where $u_x(x=0)=0$ again. Hence, we find

$$\delta = \frac{PL}{3AE_1} + \frac{2PL}{3AE_2} = \frac{PL}{3A}\left(\frac{1}{E_1} + \frac{2}{E_2}\right).$$

For the third problem (Fig. 4.6c), we must first solve the statics problem. Equilibrium of the whole requires that the reaction force R_x be given by

$$-R_x - P + 2P + P = 0 \rightarrow R_x = 2P,$$

whereas equilibrium of parts requires that we consider three separate cuts. For the first part,

$$-R_x + f(x) = 0 \rightarrow f(x) = 2P, \;\; 0 \leq x < \frac{L}{3}.$$

Similarly, for the second part,

$$-R_x - P + f(x) = 0 \rightarrow f(x) = 3P, \quad \frac{L}{3} < x < \frac{2L}{3}.$$

Finally, for the third required part,

$$-R_x - P + 2P + f(x) = 0 \rightarrow f(x) = P, \quad \frac{2L}{3} < x \leq L.$$

Indeed, the last result can be seen easily given a small part near the end. Regardless, given constants E and A and $u_x(x=0)$, we have

$$\delta = \frac{1}{AE}\left(\int_0^{L/3} 2P\,dx + \int_{L/3}^{2L/3} 3P\,dx + \int_{2L/3}^{L} P\,dx\right) = 2\frac{PL}{AE}.$$

4.1.3 Clinical Application

Now that we have some experience with the full axial load problem for LEHI behavior, let us consider an important clinical problem. Each year in the United States, ~120,000 artificial hips are implanted surgically to relieve pain and restore ambulatory motion. Figure 4.7 shows a typical prosthesis and its insertion into the host femur. As seen at Section D-D, we have nearly concentric cylindrical cross sections over part of the bone–metal interface. Although the femoral head experiences complex loads that may subject the prosthesis to compression, torsion, and bending, here let us focus on the axial load alone (other loads will be considered subsequently). This special case could be produced in the laboratory. Moreover, although the actual loads, geometry, and material properties demand a numerical (e.g., finite element) method (Fig. 4.8), let us consider a simple analysis to gain some insight into the overall problem. In particular, as a first approximation, let us assume that the bone and prosthesis each exhibit LEHI behaviors. Bone is, of course, better characterized as nonhomogeneous and anisotropic, but these simplifying assumptions have been used by many and they allow us to begin to explore the problem.

Our model problem, therefore, is simply the axial loading (through the overall centroid) of a circular cylinder consisting of two LEHI materials (Fig. 4.7b). Like most biological tissues, bone will grow and remodel in response to changes in mechanical stimuli. Therefore, one of the key questions

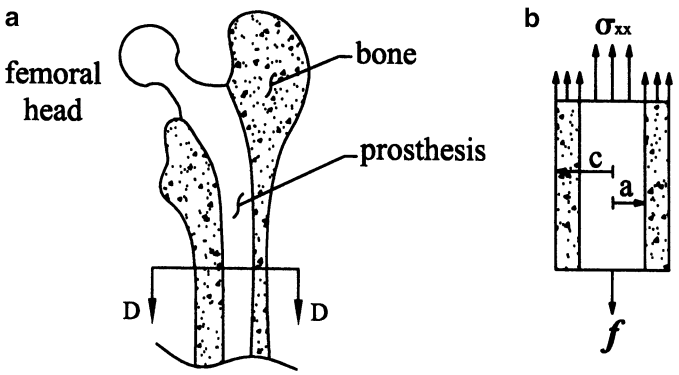

FIGURE 4.7 Schema of a metallic prosthetic hip that has been implanted to replace a damaged femoral head. One of the most common causes of femoral damage is fracture associated with osteoporosis. Defined as a reduction in bone mass, osteoporosis is a particularly debilitating disease in elderly women. If we focus on the region near Section D-D in the figure and consider the action of an axial load only, then panel **b** shows an appropriate free-body diagram for analysis to relate the axial stress to the applied loads and geometry. Although the stress may (as a first approximation) be assumed to be uniform within each constituent, metal and bone, these mean values need not be the same.

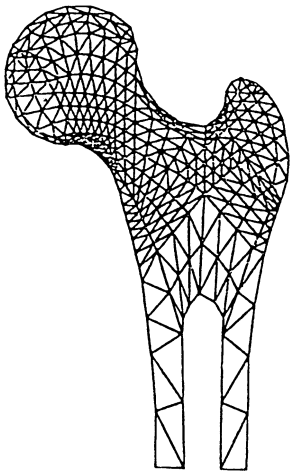

FIGURE 4.8 Illustrative finite element mesh used to analyze stresses in the femur for determining the state of stress in health, which should be mimicked as well as possible following an implant surgery. Each *triangle* represents a local computational domain, or element, in which equilibrium is enforced. Certain continuities, such as displacement, are also enforced from element to element. Albeit for a 2-D analysis of a normal femur, finite element studies can be conducted similarly in three dimensions, and for the case of a prosthesis, a poly(methyl methacrylate), or PMMA, bone cement, and bone. Finite element analyses are extremely powerful, and the student is encouraged to take at least one course in this area. With permission, from Prof. B. Simon.

with regard to prosthesis design is: How will the implant redistribute the stresses within the bone? Again, this is a complex question; we will consider the much simpler question here. On average, how does the applied load f in Fig. 4.7b distribute (i.e., partition) between the metal implant and the remaining bone? Toward this end, let the radius of the prosthesis be a and the outer radius of the bone be c. If we let that part of the load carried by the prosthesis and bone be denoted as f_p and f_b, respectively, then axial equilibrium requires that $f_p + f_b = f$. The associated mean axial stresses are thus $\sigma_{xx}^p = f_p/A_p$ for the prosthesis and $\sigma_{xx}^b = f_b/A_b$ for the bone. The key question then is: What are f_p and f_b?

With $f_p + f_b = f$, we have one equation and two unknowns, thus rendering this problem statically indeterminate; that is, we cannot determine how the load or the stress partitions using statics alone—we must seek a second equation. This can be accomplished from kinematics if we simply assume that the axial displacements are the same in each component [i.e., that there is no relative movement (e.g., delamination as discussed in Observation 2.2) between the prostheses and bone as desired of a painless implant]. Hence, if $\varepsilon_{xx}^p \equiv \varepsilon_{xx}^b$, with uniform properties along the length of the prosthesis, then we have

$$u_x(x=L)-u_x(x=0)=\int_0^L \varepsilon_{xx}^p dx=\int_0^L \frac{\sigma_{xx}^p}{E_p}dx=\int_0^L \frac{f_p}{A_pE_p}dx=\frac{f_pL}{A_pE_p}, \quad (4.7)$$

or, with $u_x(x=0)=0$,

$$\delta_p=\frac{f_pL}{A_pE_p}. \quad (4.8)$$

Similarly, for the bone,

$$u_x(x=L)-u_x(x=0)=\int_0^L \varepsilon_{xx}^b dx=\int_0^L \frac{\sigma_{xx}^b}{E_b}dx=\int_0^L \frac{f_b}{A_bE_b}dx=\frac{f_bL}{A_bE_b}, \quad (4.9)$$

or

$$\delta_b=\frac{f_bL}{A_bE_b}. \quad (4.10)$$

Hence, *to ensure compatible displacements,* $\delta_p=\delta_b$ requires that

$$\frac{f_pL}{A_pE_p}=\frac{f_bL}{A_bE_b}\rightarrow f_p=\frac{A_pE_p}{A_bE_b}f_b. \quad (4.11)$$

Thus, we have a second equation in terms of the unknown "partitioned forces." From equilibrium, we have

$$f=\frac{A_pE_p}{A_bE_b}f_b+f_b=f_b\left(1+\frac{A_pE_p}{A_bE_b}\right), \quad (4.12)$$

or

$$f_b=\frac{fA_bE_b}{A_bE_b+A_pE_p}, \quad (4.13)$$

and, similarly,

$$f_p=\frac{A_pE_p}{A_bE_b}\left(\frac{fA_bE_b}{A_bE_b+A_pE_p}\right)=\frac{fA_bE_p}{A_bE_b+A_pE_p}. \quad (4.14)$$

Finally, the stresses in the prosthesis and bone are

$$\sigma_{xx}^{p} = \frac{1}{A_p}\left(\frac{A_p E_p f}{A_p E_p + A_b E_b}\right) = \frac{E_p f}{A_p E_p + A_b E_b},$$
$$\sigma_{xx}^{b} = \frac{1}{A_b}\left(\frac{A_b E_b f}{A_p E_p + A_b E_b}\right) = \frac{E_b f}{A_p E_p + A_b E_b}. \tag{4.15}$$

We see, therefore, that the load partitions according to the respective cross-sectional areas *and* the material properties. In the special case that $E_p = E_b = E$ and $A_p + A_b = A$, we recover the original homogeneous solution ($\sigma_{xx} = f/A$), as we should. Whether the bone will resorb (atrophy) or grow will depend on whether its stress (or strain) following implantation is less than or greater than the normal physiological values. Early on, artificial implants were designed primarily to be geometrically mimicking of the native femoral head and to be strong enough that they would not fail (i.e., yield, deform plastically, or fracture; cf. Fig. 2.25) under the demands of physiological loading. Yet, the associated designs failed to consider how the stress or strain in the bone redistributed and how functional adaptation might lead to a weakening of the remaining bone over time. This flaw in the analysis and design resulted in many prosthetic failures in the early days, thus necessitating much more careful biomechanical study. The interested reader is encouraged to review the current literature on prosthesis design to appreciate the development of the field. With regard to the present (simple) analysis, a take-home message is that although we were only interested in the stresses, equilibrium alone did not permit a complete solution. This is in stark contrast to the (statically determinate) universal solutions in Chap. 3. Rather, to obtain a sufficient number of equations in this statically indeterminate problem, we sought additional equations via use of strain–displacement and stress–strain relations. We will see below and in Chap. 5 that this general approach is helpful in many different statically indeterminate problems.

4.2 Shear Stress Due to Torsion

4.2.1 Introduction

Although the analysis in Sect. 4.1.2 was restricted to LEHI material behaviors and thus small strain, there was no restriction on the cross-sectional area; that is, the developed equations held equally well for rectangular, circular, elliptical, indeed general cross sections. As we begin our study of torsion, however, the situation is very different. It has long been known that if you subject a straight member of circular cross section to a small twist, the originally parallel cross sections remain parallel. In other words, small twisting of a circular member

(shaft) does not warp the cross section. For any other cross section, such as elliptical or rectangular cross sections, torsion induces both a twist (i.e., material particles have a u_θ displacement) and a *warping motion* (e.g., u_z displacements that are nonuniform). In the next two subsections, we focus solely on small twisting motions in solid or hollow members that have a circular cross section and exhibit a LEHI behavior. As in the other problems, we will seek to relate the developed stress(es) to the applied loads and geometry [cf. Eq. (3.59)] and the deformations to the applied loads, geometry, and material properties [cf. Eqs. (3.89) or (4.5)].

4.2.2 Biological Motivation

Many biological tissues and implants are subjected to twisting loads (or torsion). Most notably, the twisting action of the heart is fundamental to the ejection of blood during each cardiac cycle; that is, consistent with Fig. 2.20, the heart shortens, constricts, twists, and shears as the muscle fibers contract during the ejection phase. In particular, the twisting action comes from a unique arrangement of the cardiac muscle fibers (Fig. 4.9), which was noticed many years ago by anatomists, but not fully appreciated until the 1970s and 1980s based on biomechanical models. It is now clear that the twisting action of the heart is not only effective in aiding the ejection of blood, it also tends to homogenize the distribution of stress across the wall of the ventricle. The latter is very important within the context of mechanobiology because a homogenized stress (or strain) field would allow the cardiac myocytes and fibroblasts to experience similar (perhaps optimal) mechanical stimuli regardless of their position within the wall of the heart. Because of the large strains and nonlinear material behavior in the heart, however, the reader is referred to Humphrey (2002) for a discussion of cardiac mechanics. Here, let us simply consider a small strain example. Figure 4.10 shows the geometry of and loads acting on the hip. Complex (compressive, bending, and twisting) loads occur naturally during daily activities as well as in the laboratory during material testing.

4.2.3 Mathematical Formulation

Recall from Sects. 3.3–3.5 that we began each stress analysis by introducing a judicious cut to isolate (or expose) the stress $\sigma_{(\text{face})(\text{direction})}$ of interest in the free-body diagram. Once done, we enforced equilibrium and related the component of stress of interest to the applied loads and geometry. Let us take the same approach here. Consider, a solid circular cylinder that is fixed on one end and free on the other; moreover, let the free end be subjected to a positive twisting moment $M_z \equiv T$ (or torque). Equilibrium of the whole (Fig. 4.11) requires an equal and opposite reaction torque T at the fixed wall, remembering,

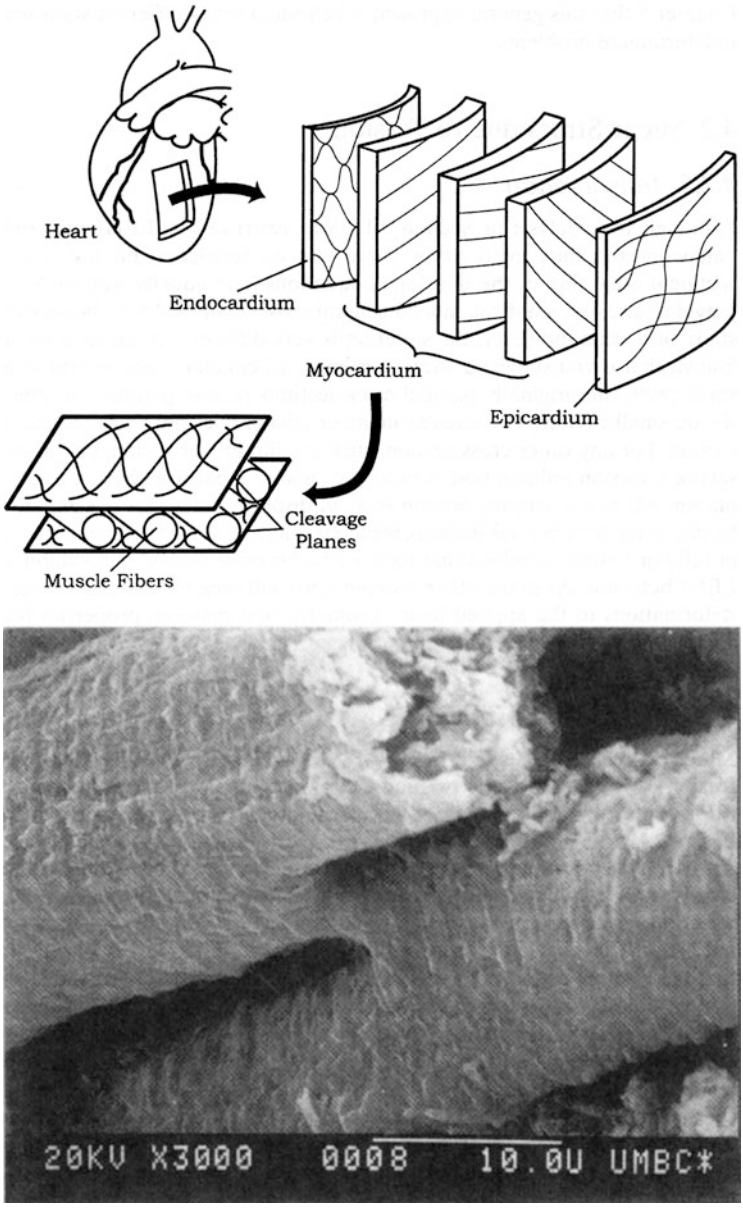

FIGURE 4.9 Schema of the heart with a cutout section from the ventricular wall showing the alternating directions of the muscle fibers (which vary smoothly throughout the wall) within the myocardium plus the delimiting connective tissue membranes on the inner (endocardial) and outer (epicardial) surfaces. The transmural splay in the muscle fibers gives rise to the twisting action of the heart upon contraction. Also shown is a scanning electron micrograph (magnification 3,000×) of two connected muscle fibers that emphasize the locally parallel structure. [From Humphrey (2002), with permission].

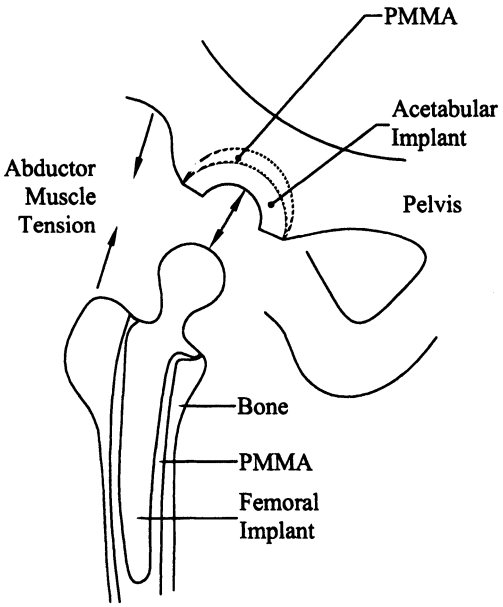

FIGURE 4.10 Schema of the femur and acetabulum, a cup-shaped cavity in which the head of the femur articulates. Because the line of action of the loads applied on the femoral head do not coincide with the long axis of the mid-shaft of the femur, these forces can cause both bending and twisting moments in addition to axial compression. Bending is addressed in Chap. 5 so we simply focus on the combined axial load and associated torque. Because of the linearity of the problem in small strain, we can use the principle of superposition and thus solve each aspect separately (compression, torsion, and bending).

of course, the right-hand rule for the positive sign convention. Next, consider equilibrium of the parts. In particular, from Fig. 4.12, we see that z-face, θ-direction stresses $\sigma_{z\theta}$ act on the cut face to balance the net applied torque T. Knowing that each $\sigma_{z\theta}$ acts over its respective differential area, with $dA = rd\theta dr$ in the circular cross section and that a torque is a force acting at a distance (i.e., a twisting moment), we must add up the effects of all stresses acting on their differential areas. Hence,

$$\sum M_z)_0 = 0 \rightarrow -T + \int_{\text{arm}} r \underbrace{\sigma_{z\theta} dA}_{df} = 0 \rightarrow T = \int_0^c \int_0^{2\pi} \sigma_{z\theta} r^2 d\theta dr. \qquad (4.16)$$

Because stress can vary from point to point, in general, we must know $\sigma_{z\theta}$ as a function of position before we can evaluate the integral. Recall that we avoided this "issue" in the axially loaded rod in Sect. 3.3 by assuming that far enough from the ends, the stress σ_{xx} was uniform (i.e., constant) over the cross section; likewise, we avoided this issue in Sects. 3.4 and 3.5 for the inflated cylinders

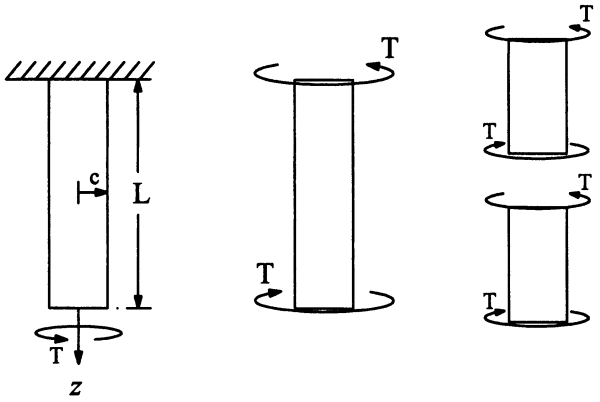

FIGURE 4.11 Schema of a solid circular cylinder (i.e., shaft) subjected to an applied torque T on the otherwise free end. (Note: The positive sign convention is consistent with the right-hand rule whereby the thumb points in the positive coordinate direction and the fingers wrap around the associated coordinate axis). Shown, too, is a free-body diagram of the whole structure to isolate the reaction at the fixed end, and a free-body diagram of two parts to isolate the internal torques. Equilibrium requires that the internal torques balance the applied and reaction torques.

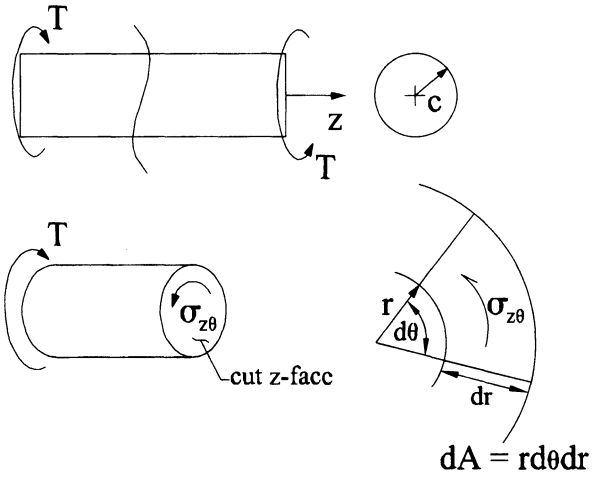

FIGURE 4.12 Alternate free-body diagram for the circular cylinder shown in Fig. 4.11, this time isolating a $\sigma_{z\theta}$ stress, on a cut z face, which serves to balance the applied torque. This balance is achieved, of course, via the net effect of all such stresses acting on their respective cross-sectional differential areas dA and at a distance from the axis called the moment arm.

and spheres by assuming thin walls and, consequently, that the stress was well represented by its mean (i.e., constant) value. Here, however, we will soon find that $\sigma_{z\theta}$ varies with radial location and that this spatial dependence cannot be ignored. Although we addressed this issue of nonuniform stress in the thick-walled cylinder in Sect. 3.6 by solving the full differential equations, here we seek an alternate, easier "strength of materials" approach. In hindsight (which means, after trying multiple approaches to no avail), it will prove convenient to employ the kinematics and constitutive relation directly.

Hence, consider the general element in Fig. 4.13 in which the angle γ is introduced to measure the circumferential motion of all material particles along a line drawn along the length of the cylinder. Moreover, let $\gamma(r = c)$ be denoted by γ_c for a line drawn on the outer surface. From trigonometry,

$$\tan \gamma_c = \frac{c\Delta\theta}{\Delta z} \quad (\text{at } r = c)$$

where

$$\lim_{\Delta z \to 0} \frac{c\Delta\theta}{\Delta z} = c\frac{d\theta}{dz} \quad (\text{at } r = c). \tag{4.17}$$

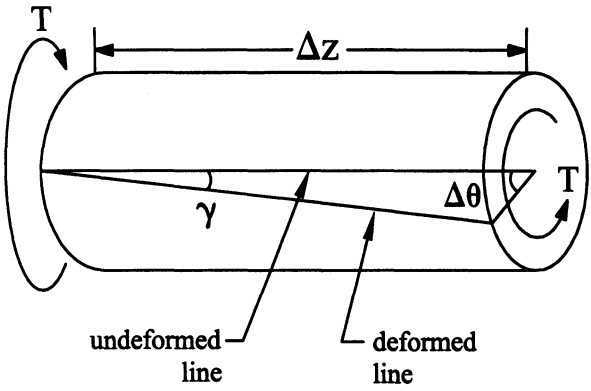

FIGURE 4.13 Schema of a circular cylinder subjected to equal and opposite end torques (assume that the torque is applied on the *right end* and that the torque at the *left end* is a reaction at a fixed boundary condition). Imagine that a straight line is drawn on the outer surface in the axial direction in the unloaded configuration. Upon the application of the torque, this line would rotate (i.e., points would displace u_θ) differently at different axial locations (cf. Fig. 2.18 for the axial load). If either the angle γ is small or the length Δz is small, then the line may be assumed to remain nearly straight and thus be describable via a single angle γ.

Next, let us restrict our attention to small changes in angles whereby the following small-angle approximation holds:

$$\tan\gamma_c \cong \gamma_c \rightarrow \gamma_c = c\frac{d\theta}{dz} \quad (\text{at } r = c). \tag{4.18}$$

Likewise, it can be shown by the same assumptions that a similar relation holds at any radius, namely

$$\tan\gamma_r \cong \gamma_r \rightarrow \gamma_r = r\frac{d\theta}{dz} \quad (\text{at any } r). \tag{4.19}$$

Having these relations, obtained from simple trigonometric arguments, we should ask: What are γ_c and γ_r? As it turns out, because of the linearization of the Green strain (Sect. 2.5), the linearized strains are related directly to small changes in length or angle; thus, γ_c and γ_r are related to a linearized shear strain. Here, ε_{zr}, $\varepsilon_{z\theta}$, and $\varepsilon_{r\theta}$ are candidate measures of shear or angle change. Of these, the strain $\varepsilon_{z\theta}$ is the measure of interest because it alone is induced by the stress $\sigma_{z\theta}$, which is needed to resist the torque T. Recall, therefore, from Hooke's Law for LEHI behavior [Eq. (2.79)] that

$$\varepsilon_{z\theta} = \frac{1}{2G}\sigma_{z\theta}, \tag{4.20}$$

where G is the shear modulus. Moreover, it can be shown that (cf. Exercise 2.27)

$$\varepsilon_{z\theta} = \frac{1}{2}(\gamma + 0) \rightarrow \gamma = 2\varepsilon_{z\theta} \tag{4.21}$$

for any r; that is,

$$\gamma_c = 2\varepsilon_{z\theta}(r = c) \text{ and } \gamma_r = 2\varepsilon_{z\theta}(r). \tag{4.22}$$

These results can be substituted into Eq. (4.20), and using Eqs. (4.18) and (4.19), we obtain

$$\begin{aligned} \sigma_{z\theta}(r) &= 2G\varepsilon_{z\theta}(r) = G\gamma_r = Gr\frac{d\theta}{dz}, \\ \sigma_{z\theta}(c) &= 2G\varepsilon_{z\theta}(c) = G\gamma_c = Gc\frac{d\theta}{dz}. \end{aligned} \tag{4.23}$$

Hindsight reveals that it is useful to take the ratio of these two stresses:

$$\frac{\sigma_{z\theta}(r)}{\sigma_{z\theta}(c)} = \frac{Grd\theta/dz}{Gcd\theta/dz} = \frac{r}{c} \rightarrow \sigma_{z\theta}(r) = \frac{\sigma_{z\theta}(c)}{c} r. \tag{4.24}$$

Whereas $\sigma_{z\theta}(r)$ is still an unknown function of radius, in general, $\sigma_{z\theta}(c)$ is just the value of this function at one point, $r = c$; hence, it is just a number. Likewise, c is just a number, the value of the outer radius; hence, via kinematics and constitutive relations, we can now evaluate the equilibrium equation (4.16):

$$T = \int \frac{\sigma_{z\theta}(c)}{c} r^2 dA = \frac{\sigma_{z\theta}(c)}{c} \int r^2 dA. \tag{4.25}$$

By recognizing the second polar moment of area (see Appendix 4) $J = \int r^2 dA$, where $dA = rd\theta dr$, we can write,

$$T = \frac{\sigma_{z\theta}(c)}{c} J \leftrightarrow \sigma_{z\theta}(c) = \frac{Tc}{J}. \tag{4.26}$$

By Eq. (4.24), however, we have

$$\sigma_{z\theta}(r) = \frac{r}{c}\frac{Tc}{J} \rightarrow \sigma_{z\theta}(r) = \frac{Tr}{J}. \tag{4.27}$$

Note, therefore, that we have succeeded in finding the stress (relative to r, θ, z) in terms of applied load (torque T) and a measure of the geometry (second polar moment of area J). This is similar to our previous (universal) results for stress in axial loading and pressurization of a thin-walled cylinder or sphere [summary in Eq. (3.59)]:

$$\sigma_{xx} = \frac{f}{A}; \quad \sigma_{\theta\theta} = \frac{Pa}{h}, \quad \sigma_{zz} = \frac{Pa}{2h} + \frac{f}{2\pi ah}; \quad \sigma_{\theta\theta} = \frac{Pa}{2h} = \sigma_{\phi\phi}.$$

There are two significant differences between the present and prior findings, however. Whereas these prior relations for stress were universal results, good for all materials, Eq. (4.27) holds only for a small-strain LEHI behavior. Moreover, in contrast to these prior results whereby the stress was uniform (i.e., independent of position within the body), Eq. (4.27) reveals a nonuniform distribution of stress; that is, the shear stress varies linearly with radial position within a circular cylinder under torsion, the stress being zero at $r = 0$ and largest at the outer radius $r = c$. Hence, if the particular "LEHI material" of interest fails due to shear, it would be expected that failure would initiate on the outer surface.

4.3 Principal Stresses and Strains in Torsion

As in Chap. 2, the components of stress at any point relative to one coordinate system can be related to those relative to another coordinate system via transformation relations like those in Eq. (2.13):

$$\sigma'_{xx} = \sigma_{xx}\cos^2\alpha + 2\sigma_{xy}\sin\alpha\cos\alpha + \sigma_{yy}\sin^2\alpha.$$

To rewrite this equation in terms of the cylindrical-polar coordinates, let $x \to z$ and $y \to \theta$; thus,

$$\sigma'_{zz} = \sigma_{zz}\cos^2\alpha + 2\sigma_{z\theta}\sin\alpha\cos\alpha + \sigma_{\theta\theta}\sin^2\alpha, \tag{4.28}$$

where α is the now the angle between z and z' and likewise between θ and θ' (recall Eq. 3.53). For members subjected to pure torsion, σ_{zz} and $\sigma_{\theta\theta}$ equal zero, thus giving the following:

$$\sigma'_{zz} = 2\sigma_{z\theta}\cos\alpha\sin\alpha. \tag{4.29}$$

By substituting Eq. (4.27) into this transformation relation, we obtain

$$\sigma'_{zz} = 2\frac{Tr}{J}\cos\alpha\sin\alpha. \tag{4.30}$$

Similarly, from Chap. 2, Eq. (2.21),

$$\sigma'_{yy} = \sigma_{xx}\sin^2\alpha - 2\sigma_{xy}\sin\alpha\cos\alpha + \sigma_{yy}\cos^2\alpha$$

can be rewritten as

$$\sigma'_{\theta\theta} = \sigma_{zz}\sin^2\alpha - 2\sigma_{z\theta}\sin\alpha\cos\alpha + \sigma_{\theta\theta}\cos^2\alpha \tag{4.31}$$

or for our case,

$$\sigma'_{\theta\theta} = -2\sigma_{z\theta}\sin\alpha\cos\alpha \to \sigma'_{\theta\theta} = -2\frac{Tr}{J}\sin\alpha\cos\alpha. \tag{4.32}$$

Finally, Eq. (2.17) can be written as

$$\sigma'_{z\theta} = \sin\alpha\cos\alpha(\sigma_{\theta\theta} - \sigma_{zz}) + \left(\cos^2\alpha - \sin^2\alpha\right)\sigma_{z\theta}, \tag{4.33}$$

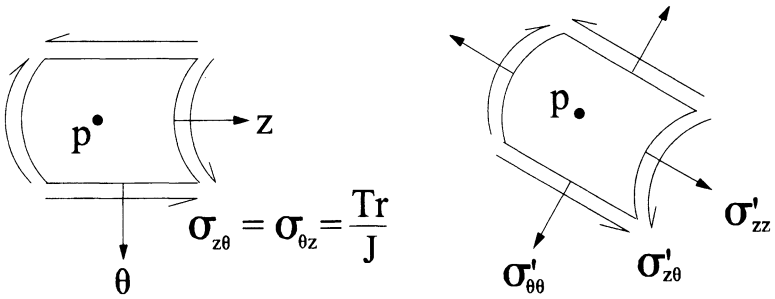

FIGURE 4.14 For pure torsion of a circular LEHI cylinder, the only nonzero component of stress at a point p is $\sigma_{z\theta}$ relative to z and θ. Relative to z' and θ' however, we may have additional components of stress, including normal and shear. We are reminded, therefore, that components of stress at a point depend on the coordinate system that is employed; they are not unique physical measurables or quantities that are "felt" directly by a cell or tissue.

or

$$\sigma'_{z\theta} = \frac{Tr}{J}\left(\cos^2\alpha - \sin^2\alpha\right). \tag{4.34}$$

See Fig. 4.14. As in Chap. 2, the principal stresses can be computed as

$$\sigma_{1,2} = \begin{cases} \sigma'_{zz})_{\max/\min} = \dfrac{\sigma_{zz}+\sigma_{\theta\theta}}{2} \pm \sqrt{\left(\dfrac{\sigma_{zz}-\sigma_{\theta\theta}}{2}\right)^2 + \sigma_{z\theta}^2} \\ \sigma'_{\theta\theta})_{\max/\min} = \dfrac{\sigma_{zz}+\sigma_{\theta\theta}}{2} \pm \sqrt{\left(\dfrac{\sigma_{zz}-\sigma_{\theta\theta}}{2}\right)^2 + \sigma_{z\theta}^2} \end{cases} \tag{4.35}$$

but for members subject to pure torsion, σ_{zz} and $\sigma_{\theta\theta}$ are zero; thus,

$$\sigma'_{zz})_{\max/\min} = \pm\sigma_{z\theta}, \quad \sigma'_{\theta\theta})_{\max/\min} = \pm\sigma_{z\theta}, \tag{4.36}$$

which is to say that the maximum/minimum normal stresses are numerically equal to the original value of the shear stress $\sigma_{z\theta}$:

$$\sigma_1 = +\frac{Tr}{J} \quad \text{and} \quad \sigma_2 = -\frac{Tr}{J}, \tag{4.37}$$

as seen in Fig. 4.15. The plane on which the maximum normal stress acts is given by an equation similar to Eq. (2.25):

$$2\alpha_p = \tan^{-1}\left(\frac{\sigma_{z\theta}}{(\sigma_{zz}-\sigma_{\theta\theta})/2}\right), \tag{4.38}$$

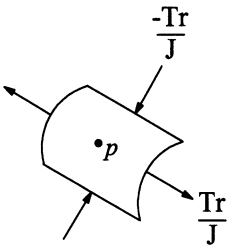

FIGURE 4.15 Principal stresses σ_1 and σ_2 at point p for the state of stress shown in Fig. 4.14. Note that the principal values are equal in magnitude but opposite in direction (i.e., one is compressive and one is tensile). Moreover, note that their magnitude is equal to the magnitude of the $\sigma_{z\theta}$ shear stress. This reminds us that components of stresses can be of the same magnitude, but different because of either the different faces on which they act or the different directions in which they act.

where σ_{zz} and $\sigma_{\theta\theta}$ are zero; hence,

$$\alpha_p = \frac{1}{2}\tan^{-1}(\infty) = \frac{\pi}{4} = 45^\circ \tag{4.39}$$

(i.e., the maximum/minimum normal stresses will act in a direction 45° from the original z or θ axis).

Similarly, the maximum shear stress can be rewritten as (from Chap. 2)

$$\sigma'_{z\theta})_{\max/\min} = \sqrt{\left(\frac{\sigma_{\theta\theta} - \sigma_{zz}}{2}\right)^2 + \sigma_{z\theta}^2} \rightarrow \sigma'_{z\theta})_{\max/\min} = \pm\frac{Tr}{J}, \tag{4.40}$$

which occurs at

$$\alpha_s = \frac{1}{2}\tan^{-1}\left(\frac{\sigma_{\theta\theta} - \sigma_{zz}}{2\sigma_{z\theta}}\right) \rightarrow \alpha_s = \frac{1}{2}\tan^{-1}(0) = 0; \tag{4.41}$$

that is, the shear stress is a maximum relative to the original (z, θ) coordinate system. Finally, note that Eqs. (4.37) and (4.40) show the maximum/minimum values relative to (z, θ) and (z', θ') coordinate systems; because the stress varies with radial direction, the largest max/min values occur at $r = c$. Hence, whether the material fails first due to shear or normal stresses, we would expect failure to initiate on the outer surface ($r = c$), in the absence of internal defects of course.

Example 4.3 A hollow LEHI cylinder has an inner radius $a = 15$ mm, an outer radius $c = 20$ mm, and a length $L = 0.5$ m. The applied torque T is 600 Nm with an angle of twist $\Delta\theta(z = L) = 3.57^\circ$. Calculate $\sigma'_{z\theta})_{\max}$ and $\sigma'_{zz})_{\max}$, find the value of the shear modulus G, and calculate $\varepsilon'_{z\theta})_{\max}$ and ε_{zz}.

Solution: From Eqs. (4.37) and (4.40),

$$\sigma'_{z\theta})_{\max} = \frac{Tr}{J} \quad \text{and} \quad \sigma'_{zz})_{\max} = \frac{Tr}{J},$$

where

$$J = \int r^2 dA = \iint r^2 r d\theta dr = \int_0^{2\pi} \int_a^c r^3 dr d\theta = \frac{\pi}{2}(c^4 - a^4).$$

Given
$a = 15\text{ mm} = 0.015\text{ m}$
$c = 20\text{ mm} = 0.02\text{ m}$
$L = 0.5\text{ m}$
$T = 600\text{ Nm}$
$\Delta\theta = 3.57^\circ = 0.0623\text{ rad}$

first calculate $\sigma'_{z\theta})_{\max}$ and $\sigma'_{zz})_{\max}$:

$$\sigma'_{z\theta})_{\max} \text{ and } \sigma'_{zz})_{\max} = \frac{Tc}{\pi(c^4 - a^4)/2} = \frac{2(600\,\text{N m})(0.02\,\text{m})}{\pi\left[(0.02\,\text{m})^4 - (0.015\,\text{m})^4\right]}$$
$$\cong 6.98 \times 10^7 \frac{\text{N}}{\text{m}^2} = 69.8\,\text{MPa}.$$

Second, calculate G. Assuming $\gamma_c \ll 1$, we have

$$\tan\gamma_c \cong \gamma_c = c\frac{d\theta}{dz} \cong c\frac{\Delta\theta}{\Delta z} = \frac{(0.02\,\text{m})(0.0623\,\text{rad})}{(0.5\,\text{m})} = 0.00249\,\text{rad}.$$

Hence, $\sigma_{z\theta}(r = c) = 2G\varepsilon_{z\theta}(r = c) = G\gamma_c$ implies that

$$G = \frac{\sigma_{z\theta}}{\gamma_c} = \frac{6.98 \times 10^7\,\text{N/m}^2}{0.00249} = 2.80 \times 10^{10}\text{Pa} = 28.0\ \text{GPa}.$$

Third, calculate $\varepsilon'_{z\theta})_{\max}$ and ε_{zz} using Hooke's law:

$$\varepsilon'_{z\theta})_{\max} = \frac{1}{2G}\sigma'_{z\theta})_{\max} = \frac{69.8\,\text{MPa}}{2(28.0\,\text{GPa})} = 0.00125$$

and, finally,

$$\varepsilon_{zz} = \frac{1}{E}[\sigma_{zz} - \nu(\sigma_{rr} + \sigma_{\theta\theta})] = 0.$$

Thus, the shaft does not extend and the maximum shear strain is indeed small, consistent with our small-strain assumption in the derivation of the governing equations and our use of a LEHI descriptor of the behavior. Also note that in reference to Table A2.1, a shear modulus $G \sim 28$ GPa suggests that the material is a 2024-T4 aluminum. The yield strength of this material is ~170 MPa in shear; hence, we would not expect that yield would have occurred.

Example 4.4 A solid circular member is to be subjected to an applied torque of 500 Nm. Find the required diameter of the member so as not to exceed the maximum stress $\sigma_{z\theta}$ of 125 MPa.

Solution: Given

$$\sigma_{z\theta} = 125, \text{MPa} = 1.25 \times 10^8 \frac{\text{N}}{\text{m}^2}, \quad T = 500 \text{ Nm};$$

let the maximum radius $r = c$. From Eq. (4.27),

$$\sigma_{z\theta} = \frac{Tr}{J} \quad \text{or} \quad \sigma_{z\theta}(r = c) = \frac{Tc}{J},$$

where

$$J = \int r^2 dA = \iint r^2 r d\theta dr = \int_0^{2\pi} \int_0^c r^3 dr d\theta = \frac{\pi}{2} c^4.$$

Hence,

$$\sigma_{z\theta}(c) = \frac{Tc}{(\pi/2)c^4} = \frac{2T}{\pi c^3} \rightarrow c^3 = \frac{2T}{\pi \sigma_{z\theta}} \rightarrow c = \left(\frac{2T}{\pi \sigma_{z\theta}} \right)^{1/3},$$

or

$$c = \left(\frac{2(500 \text{Nm})}{\pi (1.25 \times 10^8 \text{N/m}^2)} \right)^{1/3} = 0.0137 \text{m} = 13.7 \text{mm},$$

and thus the minimum allowable diameter is $2c = 27.4$ mm, which is just over 1 in.

Observation 4.2. Not all bones serve the same function. Some serve primarily to protect underlying soft tissue (e.g., the skull and sternum); thus, they have significant strength but carry little load most of the time. Conversely, other

bones serve intermittently as load-bearing structures (e.g., the humerus, radius, and ulna of the arm), whereas still others consistently bear significant loads (e.g., the spine as well as the femur, tibia and fibula of the leg). We would expect, therefore, that the strains experienced by these different bones differ significantly throughout a normal day. Much of the attention in the mechanobiology of bone has focused on load-bearing long bones.

Regardless of their primary function, from the perspective of mechanics, bones tend to experience small strains. Hence, given that bones are also relatively stiff, standard strain gauges can be used to measure the surface strains that they experience under either in vitro or in vivo loading conditions. Given material properties, of course, stresses can then be computed from measured strains without the need to solve the equilibrium problem (for that point). Note, therefore, that the magnitude of peak *compressive* strains measured in vivo on the outer surface of load-bearing bones (e.g., cortical bone of the diaphysial region of the femur) have been reported on the order of 0.001 or less during normal walking (often ~0.0004) and between 0.002 and 0.004 during vigorous exercise. It is interesting to note, therefore, that Rubin and Lanyon (1985) reported a maintenance of cortical bone (i.e., a balanced production by osteoblasts and removal by osteoclasts) when the compressive strain is between 0.0005 and 0.0015. Above a strain of ~0.0015, there tends to be a net growth whereby production exceeds removal. Microdamage may occur, however, when the strains are greater than 0.0025 in tension or 0.004 in compression. Microdamage is also thought to stimulate a bone growth/healing response. Yield may occur at strains of ~0.006 in tension and 0.009 in compression, whereas cracks can occur when strains exceed ~0.03, which will also elicit a bone growth/healing response. Of course, sustained inactivity (e.g., bedridden patients) or gross unloading (e.g., in astronauts in a microgravity environment) leads to a net loss of bone material in bones that normally support loads. We conclude, therefore, that consistent, vigorous exercise promotes bone growth by increasing the strains (or stresses) and, through mechanotransduction mechanisms, increasing the production and organization of bone material by the osteoblasts. Let us now look at small strain deformations in torsion, one load seen daily by bones such as the femur.

4.4 Angle of Twist Due to Torque

Recall from Sect. 4.1 that in axial load problems, it is often useful to find the maximum displacement (extension), denoted as δ, as well as the displacement vector and strain fields. So, too, with torsion, it is often useful to determine the maximum angle of twist

$$\Theta = \int \frac{d\theta}{dz} dz \quad \text{at } r = c. \tag{4.42}$$

4.4.1 Basic Derivation

From Eqs. (4.19)–(4.21), we recall that

$$\gamma_r = r\frac{d\theta}{dz}, \quad \varepsilon_{z\theta} = \frac{1}{2}\gamma_r, \quad \varepsilon_{z\theta} = \frac{1}{2G}\sigma_{z\theta}. \tag{4.43}$$

Hence, from Eq. (4.27), we have

$$\frac{d\theta}{dz} = \frac{1}{r}\gamma_r = \frac{1}{r}2\left(\frac{1}{2G}\sigma_{z\theta}\right) = \frac{1}{rG}\left(\frac{Tr}{J}\right) = \frac{T}{JG}, \tag{4.44}$$

and, consequently, the angle of twist Θ can be computed via

$$\Theta(z) - \Theta(0) = \int_0^z \frac{d\theta}{dz} dz = \int_0^z \frac{T(z)}{J(z)G(z)} dz, \tag{4.45}$$

where, similar to Eq. (4.5), we allow the torque, second polar moment of (cross-sectional) area, and shear modulus to vary with position z along the length in general. It is important to note, therefore, that if the shaft is homogeneous, then $G \neq G(z)$; if the shaft has a constant cross-sectional area, then $J \neq J(z)$; and if the shaft is under a constant torque, then $T \neq T(z)$. The direction of the angle of twist Θ coincides with the direction of the applied torque T.

Example 4.5 Find the total twist at a distance z in each of the members in Figs. 4.16 and 4.17.

Solution:

$$\Theta(z) - \Theta(0) = \int_0^z d\theta, \quad d\theta = \frac{T}{JG} dz.$$

The first shaft is homogeneous and acted upon by a constant torque; it does not have a constant cross-sectional area however. The area changes from A_1 to A_2 at a length of $L/2$ from the wall. Therefore, $J = J(z)$ and the angle of twist becomes

$$\Theta(L) - \Theta(0) = \int_0^L \frac{T}{J(z)G} dz = \frac{T}{G}\int_0^{L/2} \frac{1}{J_1} dz + \frac{T}{G}\int_{L/2}^L \frac{1}{J_2} dz.$$

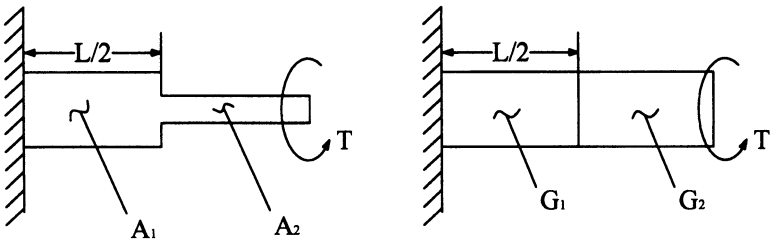

FIGURE 4.16 Two idealized circular cylinders of length L are acted upon by a single, constant end torque T. The cylinder on the *left* has a nonconstant cross section, whereas the one on the *right* is nonhomogeneous in composition.

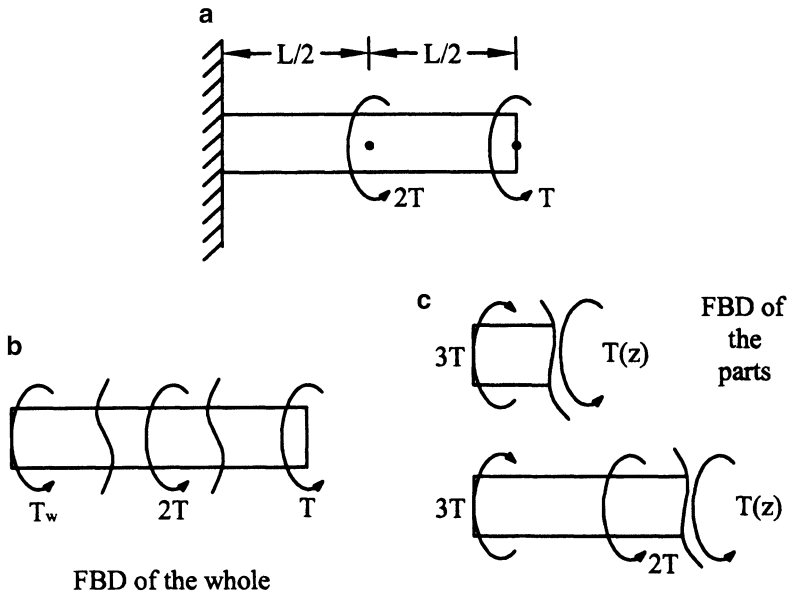

FIGURE 4.17 A LEHI circular cylinder subjected to multiple applied torques. A free-body diagram of the whole allows the reaction support T_w to be determined; free-body diagrams of judiciously selected parts allows internal torques to be determined as a function of z. Remember that judicious cuts are typically those taken between abrupt changes in applied loads.

Because the integral was broken into a sum of integrals for the discontinuity in cross-sectional area, each new integral contains terms that are constant along the range of integration and can be moved outside the integral and evaluated. Given that the twist at the fixed end is zero [i.e., $\Theta(0) = 0$], we have

$$\Theta(L) - \Theta(0) = \frac{T}{J_1 G}\int_0^{L/2} dz + \frac{T}{J_2 G}\int_{L/2}^{L} dz \rightarrow \Theta(L) = \frac{TL}{2J_1 G} + \frac{TL}{2J_2 G}.$$

The second shaft has a constant cross-sectional area and is acted on by a constant torque; it is not homogeneous however. The material properties change at a distance of $L/2$ from the wall. Therefore, $G = G(z)$ and the twist becomes

$$\Theta(L) - \Theta(0) = \int_0^L \frac{T}{JG(z)} dz = \frac{T}{J}\int_0^{L/2} \frac{1}{G_1} dz + \frac{T}{J}\int_{L/2}^{L} \frac{1}{G_2} dz,$$

or

$$\Theta(L) = \frac{TL}{2J}\left(\frac{1}{G_1} + \frac{1}{G_2}\right).$$

The third shaft is homogeneous and has a constant cross-sectional area; it is not under a constant loading however. The applied load changes at a distance of $L/2$ from the wall; thus, $T = T(z)$. Before we solve for the twist at the end of the shaft, we must determine the internal torques at each z. From equilibrium of the whole (Fig. 4.17b), we see that the reaction torque at the wall T_w must balance the combined effects of the $2T$ and the T that are applied at $z = L/2$ and $z = L$, respectively. Equilibrium of parts (note: when we have discrete changes in loads, geometry, or properties, judicious cuts are those between the abrupt changes) reveals further that the left half has an internal torque $3T$ and the right half only T. Hence, the end twist becomes

$$\Theta(L) - \Theta(0) = \frac{3T}{JG}\int_0^{L/2} dz + \frac{T}{JG}\int_{L/2}^{L} dz \rightarrow \Theta(L) = \frac{3TL}{2JG} + \frac{T}{JG}\left(\frac{L}{2}\right) = 2\frac{TL}{JG}.$$

4.4.2 Statically Indeterminate Problems

Just as in the case of the axially loaded rods, cases in which we do not have a sufficient number of equations from statics for the number of unknowns arise naturally and frequently in torsion problems. Such cases are called *statically indeterminate* because all quantities cannot be determined from statics alone. Here, let us return to the bone–prosthesis experiment of Sect. 4.1.3, but now focus on shear stresses induced by torsion. Referring to Fig. 4.18, we know that if we assume separate LEHI behaviors for the prosthesis and bone that

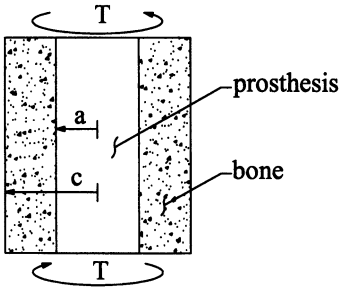

FIGURE 4.18 Similar to Figure 4.7, at section D-D, except that the bone-prosthesis system is subjected to a constant end torque T (i.e., a twisting moment having units of force times length).

$$\sigma_{z\theta}^{p} = \frac{T_p r}{J_p}, \quad 0 \le r < a, \quad \text{and} \quad \sigma_{z\theta}^{b} = \frac{T_b r}{J_b}, \quad a < r \le c, \tag{4.46}$$

where T_p and T_b are those portions of the overall torque T carried by the prosthesis and bone, respectively, and

$$J_p = \frac{\pi}{2}a^4, \quad J_b = \frac{\pi}{2}\left(c^4 - a^4\right). \tag{4.47}$$

From equilibrium, we know that $T = T_p + T_b$, but we do not yet know how the torque partitions. For a painless prosthesis, we require that there be no relative motion and, consequently, that all overall rotations, including the total end rotation, be equal; that is,

$$\Theta_p = \frac{T_p L}{J_p G_p} = \frac{T_b L}{J_b G_b} = \Theta_b \rightarrow T_p = \frac{T_b J_p G_p}{J_b G_b}, \tag{4.48}$$

which, with $\Theta(0) = 0$, yields our second equation for our second unknown. Hence,

$$T_b = \frac{T J_b G_b}{J_b G_b + J_p G_p}, \quad T_p = \frac{T J_p G_p}{J_b G_b + J_p G_p}, \tag{4.49}$$

and, therefore,

$$\begin{aligned} \sigma_{z\theta}^{p} &= \frac{T G_p r}{J_b G_b + J_p G_p}, \quad 0 \le r < a, \\ \sigma_{z\theta}^{b} &= \frac{T G_b r}{J_b G_b + J_p G_p}, \quad a < r \le c. \end{aligned} \tag{4.50}$$

In summary, we see again that if statics alone does not provide sufficient information, we should appeal to remaining equations (e.g., kinematics, constitutive, and boundary conditions).

Example 4.6 Consider the simple shaft shown in Fig. 4.19, which has uniform LEHI properties and is fixed on both ends. Find the torque T in each section.

Solution: Because the shaft is fixed at both ends, the problem is statically indeterminate. If we let the end torques be denoted by T_A and T_C, overall equilibrium requires that $T_o + T_C + T_A = 0$ (where T_o is the known, applied torque). We need another equation to find the reactions however. Note, therefore, that

$$\Theta(L/2) - \Theta(0) = \int_0^{L/2} -\frac{T_A}{J_1 G} dz = -\frac{T_A L}{2J_1 G}, \quad \Theta(L) - \Theta(L/2) = \frac{T_C L}{2J_2 G}$$

where $\Theta = 0$ at both $z = 0$ and $z = L$. Moreover, $\Theta(L/2)$ is but a single value; thus,

$$\Theta(L/2) = -\frac{T_A L}{2J_1 G} = -\frac{T_C L}{2J_2 G} \rightarrow T_A = T_C \frac{J_1}{J_2}$$

and therefore, having two equations and two unknowns, we can solve for the two reactions

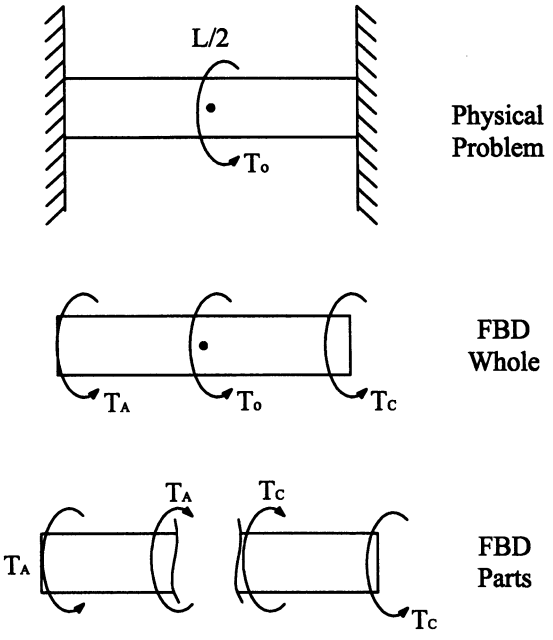

FIGURE 4.19 Statically indeterminate shaft, fixed on both ends, and subjected to a single applied torque T_o at $z = L/2$. Free-body diagrams of the whole structure and the parts allow the reaction and internal torques to be isolated but not determined because we have only one nontrivial equation (the sum of the twisting moments equals zero) for the two reaction torques T_A and T_C. There is, therefore, a need for an additional equation.

$$T_C = -T_o\left(\frac{J_2}{J_1 + J_2}\right), \quad T_A = -T_o\left(\frac{J_1}{J_1 + J_2}\right).$$

As a special case, note that if $J_1 = J_2$ (i.e., the shaft has a constant cross section), then $T_C = -T_o/2$ and $T_A = -T_o/2$, as expected.

Observation 4.3. One of the main complications with metallic implants (i.e., prostheses) is a gradual loosening of the device over time. Although infection and the associated degradation of bone material can cause loosening, aseptic loosening (i.e., mechanical failure) remains the most common cause of failure. PMMA, or poly(methyl methacrylate), is commonly used as a cement to fix metallic implants within bone. Because loosening is often due to the development of microcracks within the PMMA, there is a need to understand the associated mechanics. PMMA has a stiffness (i.e., Young's modulus) of 2–3 GPa, a Poisson's ratio of 0.35, a mass density of 1,220 kg/m^3, a yield stress of about 28 MPa, and a tensile strength of about 83 MPa. Tensile strength is the maximum stress attained by a material on a σ versus ϵ curve. A particularly important characteristic, however, is the *fracture toughness* of the PMMA bone cement (i.e., its ability to withstand applied loads in the presence of flaws, including cracks). Whereas the load-carrying capability of a material containing defects or cracks is not compromised much in compression, which tends to close the defect, the behavior in tension and shear is very important. Indeed, excessive shear stresses at the bone–cement interface are thought to play a key role in the loosening of a hip implant.

A typical fracture toughness test consists of applying known axial stresses on a uniaxial sample that has a well-defined flaw in the central region (Fig. 4.20); this flaw experiences increased stress at its tip, which serves to nucleate and possibly to propagate a crack. For this simple test, a stress intensity factor K is often defined as $K = f\sigma\sqrt{\pi a}$, where f is a geometric factor for the specimen and flaw, σ is the applied axial stress, and a is a measure of the width of the flaw. The critical value of K at which the flaw begins to propagate is known as the fracture toughness K_c. Values of K_c for PMMA are around $990\,\text{MPa}\sqrt{\text{m}}$. Whereas increased rates of loading or the presence of large defects reduce the fracture toughness, increasing the presence of very small inclusions tends to increase K_c. Such inclusions, including grains in metals, tend to arrest the propagation of a microcrack because more energy is needed to divert the crack around the inclusion. For this reason, small whiskers of titanium are sometimes added to the bone cement. These whiskers not only increase the fracture toughness of the bone cement, they also improve its radio-opacity and thus permit an easier examination of the integrity of the cement with X-rays. We have not considered fracture mechanics or the associated material science herein, but the student must know that many real life problems require advanced methods and the

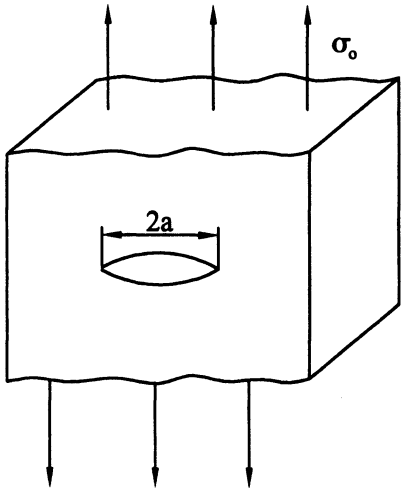

FIGURE 4.20 Schema of a specimen used for determining the fracture toughness of a material.

expertise of many to understand fully the clinical problem and its most effective solution. We emphasize again, therefore, that this text is but an introduction; the interested student must pursue advanced courses in applied mechanics and biomechanics.

4.5 Experimental Design: Bone Properties

We recall from Chap. 2 that bones are typically heterogeneous (cortical and cancellous bone being very different); here, we consider a simple experiment to determine a first-order approximation for the shear modulus G in the diaphysial region of the femur based on the assumptions of homogeneity and isotropy. Pretend, however, that we do not have access to a tension–torsion device, which would allow us to perform a torsion test on a cylindrical sample and thereby to measure the end rotation $\Theta(z = L)$, applied torque T_o, length L, and second polar moment of area J that are needed to calculate $G = TL/J\Theta$. Rather, assume that we have available a much less expensive axial load device. We are thus faced with the dilemma of determining the value of the shear modulus G via an axial load experiment; let us employ our theoretical framework for help.

Actually, there are various ways to overcome this problem. First, we could recall that for isotropy, $G = E/2(1 + \nu)$ and therefore we simply need to determine E and ν. If we perform a uniaxial load test, we can infer σ_{xx} and ε_{xx} (with $\sigma_{xx} = E\varepsilon_{xx}$) from measurables: $\sigma_{xx} = f/A$, which can be determined by measuring the applied load and the cross-sectional area, and ε_{xx}, which can be obtained directly from an axially oriented strain gauge (because the bone will experience

small strains in its elastic range). Indeed, if $\varepsilon_{xx} \equiv \varepsilon_{\text{axial}}$, then a second strain gauge placed orthogonal to the first would yield $\varepsilon_{\text{lateral}}$ whereby

$$G = \frac{E}{2(1+\nu)} = \frac{\sigma_{xx}/\varepsilon_{xx}}{2(1-\varepsilon_{\text{lateral}}/\varepsilon_{xx})} = \frac{f/A\varepsilon_{\text{axial}}}{2(\varepsilon_{\text{axial}}-\varepsilon_{\text{lateral}})/\varepsilon_{\text{axial}}}, \tag{4.51}$$

or

$$G = \frac{f}{2A(\varepsilon_{\text{axial}}-\varepsilon_{\text{lateral}})}. \tag{4.52}$$

Alternatively, we could recall our transformation equations for stress and strain (Chap. 2). For example,

$$\sigma_{xy}^{'})_{\max} = \sqrt{\left(\frac{\sigma_{xx}-\sigma_{yy}}{2}\right)^2 + \sigma_{xy}^2}, \quad \varepsilon_{xy}^{'})_{\max} = \sqrt{\left(\frac{\varepsilon_{xx}-\varepsilon_{yy}}{2}\right)^2 + \varepsilon_{xy}^2}, \tag{4.53}$$

where, for a uniaxial test, $\sigma_{yy} = 0$, $\sigma_{xy} = 0$, and $\varepsilon_{xy} = 0$. Thus, we simply need to invoke the constitutive relation relative to the primed coordinates, namely

$$\sigma_{xy}^{'})_{\max} = 2G\varepsilon_{xy}^{'})_{\max} \rightarrow G = \frac{1}{2}\frac{\sigma_{xx}/2}{(\varepsilon_{xx}-\varepsilon_{yy})/2}, \tag{4.54}$$

or with $\sigma_{xx} = f/A$, $\varepsilon_{xx} \equiv \varepsilon_{\text{axial}}$, and $\varepsilon_{yy} \equiv \varepsilon_{\text{lateral}}$,

$$G = \frac{f}{2A(\varepsilon_{\text{axial}}-\varepsilon_{\text{lateral}})}, \tag{4.55}$$

which is the same result as obtained earlier. We see again, therefore, that theory helps us to determine what to measure—that is to say, how to design a good experiment. If we were working in industry, our boss would be particularly pleased if our knowledge of theory would allow the desired result (here, the value of G) to be determined using available instrumentation (a standard axial load frame) rather than necessitating the expense and delay associated with the purchase of more specialized equipment.

4.6 Experimental Design: Papillary Muscles

4.6.1 Biological Motivation

The wall of the heart consists primarily of myocardium, which is delimited on its inner and outer surfaces by thin endocardial and epicardial membranes (Fig. 4.9). Whereas these delimiting membranes consist primarily of a 2-D

plexus of collagen with admixed elastin, the myocardium consists primarily of locally parallel cardiomyocytes that are embedded in a 3-D collagenous matrix. Clearly, then, the myocardium and delimiting membranes exhibit very different mechanical behaviors (recall Fig. 2.24) consistent with their very different biomechanical functions. Fundamental to understanding overall cardiac function, therefore, is a detailed knowledge of the mechanical properties of the various tissues that constitute the heart. Quantification of the mechanical properties of the myocardium is complicated, however, by its ability to contract as a muscle and the observation that it experiences multiaxial finite extensions, shortening, and shears throughout the normal cardiac cycle (recall Fig. 2.20). There is a need, therefore, for tests that address both of these complexities.

The papillary muscles are thin, fingerlike projections within the ventricles of the heart (cf. Fig. 3.2). They consist of locally parallel myocardial fibers that are oriented along the axial direction, plus a thin delimiting endocardial membrane. Because some papillary muscles (e.g., from the right ventricle of the rabbit) are thin, nearly circular in cross section, and of modest taper along a significant portion of their length, they have proven to be ideal specimens for experiments that seek to quantify behavior in extension (i.e., axial loading) and shear (i.e., torsion) in both active and passive states; that is, the thinness of such specimens allows one to induce muscular contraction by bathing the papillary muscle in an appropriate solution, such as a normal physiologic solution augmented with barium to induce contracture or, likewise, to induce relaxation by changing the bathing solution to one containing an appropriate cardioplegic (e.g., high potassium and 2,3-butanedione 2-monoxime, or BDM). From the perspective of mechanics, therefore, one can design a tractable experiment: the combined axial extension and torsion of a cylindrical specimen having either active or passive properties. Given that we have derived formulas for axial extension and torsion, it may seem that it would be easy to design and interpret such an experiment to determine the stress–strain behavior of a papillary muscle and, thus, myocardium. Here, however, *we must be very careful*: Whereas the formula for Cauchy stress in an axially loaded member ($\sigma_{zz} = f/A$) is a universal solution and thus applicable to any material and any degree of strain, the analogous formula for Cauchy stress in the torsion of a circular member ($\sigma_{z\theta} = Tr/J$) holds only for LEHI behavior and small strains. Likewise, the formulas for end deflection (e.g., $\delta = fL/AE$) and that for end rotation ($\Theta = TL/JG$) are both restricted to small strains. The characteristic nonlinear, inelastic, heterogeneous, and anisotropic behavior exhibited by myocardium thus prohibits the use of three of our otherwise four seemingly applicable formulas.

Although we discuss some aspects of the quantification of nonlinear material behavior in Chap. 6, here let us see that how our simple results can still be used to design an appropriate experiment on a complex soft tissue.

4.6.2 *Experimental Design*

Consider Fig. 4.21, which illustrates a possible setup for an extension–torsion test on a papillary muscle. In particular, we need actuators to induce both extension and torsion; this can be accomplished with computer-controlled stepper motors, which are commercially available at the appropriate resolution in motion. We also need a method to measure the strain in the central region; although standard strain gauges cannot be used, strains can be inferred by affixing small markers to the surface of the specimen and tracking their motion with a video camera and computer image analysis system. From marker displacements, of course, we can compute the requisite displacements and their gradients (by introducing interpolation functions) to compute surface strains as discussed in Chap. 2. Although papillary muscles are small and thus subject to relatively small axial loads, commercial load cells are available with the requisite resolution. Measurement of the applied torque is not so simple

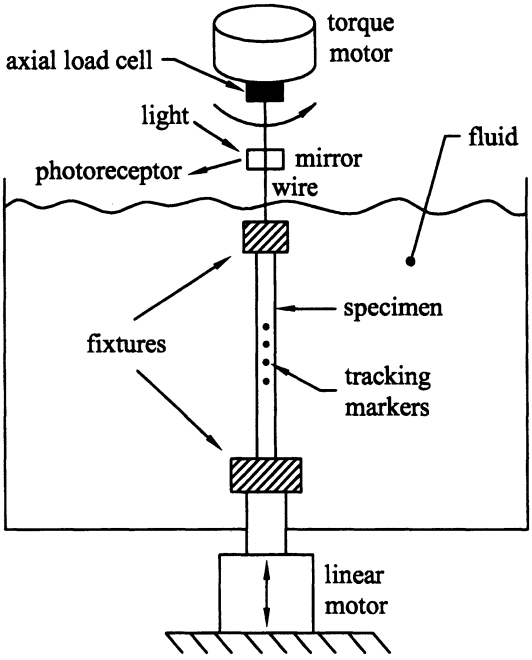

FIGURE 4.21 Possible experimental setup for performing an extension–torsion test on a thin, long, circular soft tissue. Shown are two actuators (a linear motor and torque motor to induce the extension and twisting, respectively), a standard axial load cell, a custom laser lever for measuring the torque, and a specimen in a physiologic solution. Note that the specimen has markers affixed to its surface to allow noncontacting measurements of displacements and then, via interpolation, calculation of displacement gradients and thus strains.

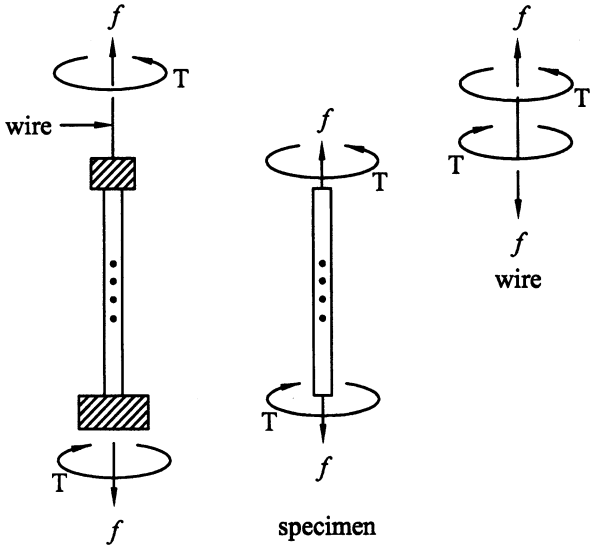

FIGURE 4.22 Free-body diagrams of the specimen–fixture assembly for the device in Fig. 4.21 as well as of the isolated specimen and the wire that connects the upper fixture to the torque motor. Although the metallic wire and soft tissue have very different material properties (recall Fig. 2.23), equilibrium and Newton's third law require continuity in the applied loads from one to the other.

however because a torque is a force acting at a distance. For a papillary muscle from the right ventricle (RV) of the rabbit or rat heart, this means a small force acting at a very small distance; hence, the applied torque will be very small. Therefore, let us see how the results of this chapter can be used to design an appropriate torque transducer.

Figure 4.22 is a free-body diagram of the bottom fixture, specimen, upper fixture, and thin connecting wire assembly. Because equilibrium of the whole implies equilibrium of the parts, each member of this assembly has a similar free-body diagram. In particular, there must be continuity of the applied loads throughout each member of this specimen–fixture assembly. In other words, if we can measure the torque acting on either the bottom or the upper fixture, we will know the torque that acts on the papillary muscle. In a Ph.D. dissertation, Sten-Knudsen (1953) recognized this and suggested that the upper fixture be connected to a thin metallic wire that exhibits a LEHI behavior. Consequently, if one measures the rotation at two points along the wire, say Θ_A and Θ_B, and if one knows the radius c and the shear modulus G of the wire, then the torque on the wire is [from Eq. (4.45)]

$$T = \frac{(\Theta_B - \Theta_A)JG}{L}, \quad J = \frac{\pi}{2}c^4, \tag{4.56}$$

where Θ_A and Θ_B are the rotations at points A and B and L is the distance between A and B. If the load cell in Fig. 4.22 is rigidly attached to the torque motor, then Θ_A simply equals the rotation of the torque motor, which is generally available as a digital output signal. How then do we measure Θ_B? One possibility is to measure the angle of reflection of a beam of light (i.e., a laser) using a mirror that is attached rigidly to the wire at B and a photoreceptor. The resolution and range of the torque transducer is thus controlled largely by the position of the mirror at B, the radius of the wire, and the shear modulus of the wire G. Each of these quantities are easily measured.

In summary, we sought a tractable experiment to reveal the nonlinear extensional and shear behaviors of myocardium in active and passive states. Nature provided a nearly ideal sample in the thin and nearly circular papillary muscle. Whereas commercially available stepper motors, video cameras, frame-grabber boards, axial load cells, and A/D boards allow one to control and measure most of the requisite quantities, the unavailability of a commercial torque transducer having sufficient resolution (in 1953 and today) necessitated a custom design. We saw, therefore, that our simple strength of materials solution restricted to LEHI behavior could be used to design such a transducer for measuring torques in a tissue that exhibits a nonlinearly, inelastic, heterogeneous, and anisotropic material behavior. Knowing not only the restrictions but also the applications of each derivation is thus fundamental to creative analysis and design. Whereas we have considered only the design of the transducer here, Humphrey (2002) addressed the complete problem via nonlinear mechanics.

4.7 Inflation, Extension, and Twist

Because the stress boundary value problems associated with the distension of a thin-walled circular tube, the small strain axial extension of a rod, and the small strain twist of a circular shaft are each linear, their solutions can be superimposed to consider more complex loading conditions. In particular, relative to (r, θ, z) coordinates, recall the following results:

$$\sigma_{\theta\theta} = \frac{Pa}{h}, \quad \sigma_{zz} = \frac{Pa}{2h} + \frac{f}{2\pi ah}, \quad \sigma_{z\theta} = \frac{Tr}{J} \tag{4.57}$$

wherein we emphasize that each result relates the stress to the applied load and geometry. Referring to Fig. 4.23, therefore, we see a potentially complex 2-D state of stress. From a design perspective, one could ask questions such as: What are the maximum principal or shear stresses and at what orientation α do they

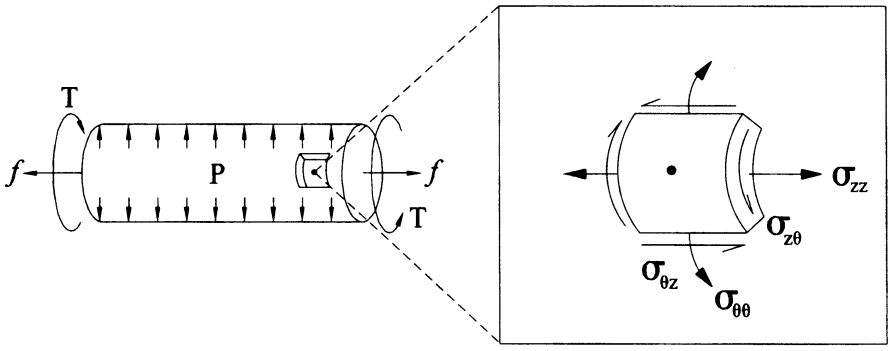

FIGURE 4.23 Complex state of stress in a cylindrical tube. Relative to z and θ, the axial stress σ_{zz} is induced by the axial load f, the shear stress $\sigma_{z\theta}$ is induced by the torque T, and the circumferential stress $\sigma_{\theta\theta}$ is induced by the pressure P. Superposition applies because the problem is linear.

act? Knowing the value α_p for the principal values would be useful, for example, in the placement of strain gauges on the specimen. Fortunately, such questions are answered easily because the formulas for stress in Eq. (4.57) can be superimposed.

In summary, as we noted in the Introduction, considering separately the mechanics of simple problems not only gives us intuition and reinforces the general method of approach, it also yields direct applications and in some cases it allows us to consider more complex situations consisting of multiple types of applied load. In any event, we must always be mindful of the derivations (i.e., of the embodied assumptions).

Chapter Summary

This chapter addresses, in part, two of five aforementioned canonical problems in biosolid mechanics: extension of 1-D structures and torsion of cylindrical structures. The other canonical problems are considered in Chaps. 3 and 5. Obvious applications of solutions to extension and torsion problems include the analysis of bones, tendons, ligaments, and muscles, but many others as well, including diverse experimental fixtures or medical devices. As in Chap. 3, we sought to determine stress in terms of the applied load and geometry and to determine strain, or associated deformations, in terms of the applied load, geometry, and material properties.

Although stress in an axially loaded, uniform 1-D structure (Sect. 3.3) can be determined via a universal solution (i.e., independent of constitutive properties), we found in this chapter that determination of the associated strain required specification of a constitutive relation (Eq. 4.4). Hence, even for the

same problem, one must be careful to remember the limitations of individual results. Indeed, in many books one finds that stress and strain in axial loading are derived in the same section without emphasizing that the solution for stress is universal whereas that for strain is not. This observation is especially important to remember given that years from now the reader may need to use such solutions, but will likely only look in the index to find the associated result (e.g., Eqs. 3.29 and 4.4) without reviewing the individual derivations. The importance of remembering limitations of results cannot be over-emphasized.

We also found that determination of stresses in an axially loaded, composite 1-D structure required information on the constitutive behavior via the *kinematic constraint* of compatible displacements (i.e., the problem was statically indeterminate and thus required additional equations). Hence, even for the same class of problems, universal solutions may or may not exist depending on slight differences. Remembering the solution methodology and associated assumptions is thus critical.

The solution for shear stress in a uniform, solid cylinder (e.g., 4.27) yielded the desired result: stress in terms of applied load (i.e., the torque, or twisting moment T) and geometry (radial location r and the second polar moment of area J). Although material properties (e.g., shear modulus G) do not appear explicitly in this final relation, the solution is nevertheless not universal. As revealed by the derivation, material properties had to be introduced (cf. Eq. 4.20, Hooke's law for LEHI behavior in shear). Again, therefore, we must be mindful of the derivation and inherent limitations of each result. Comparable results for stress for a composite, solid cylinder (Eq. 4.50) as well as those for the deformation of even a uniform cylinder (cf. Eq. 4.45) reveal directly the restriction to a particular constitutive behavior.

Although defining a cylindrical coordinate system aligned with the long axis of a cylinder is clearly advantageous in the solution of these problems involving extension and torsion, we recall that the resulting components of stress or strain need not be the most useful with regard to understanding either material failure or mechanobiological responses. That is, as noted in Chap. 2, components of stress and strain exist relative to coordinate systems that we select, thus we should first select that system which is most convenient for solving the overall initial or boundary value problem. Once accomplished, we should then use transformation relations (Chap. 2) as needed to consider other components of interest, including but not limited to principal values, which might be more relevant to the material science or the biology.

Finally, Sects. 4.5 and 4.6 remind us that solutions for stress and strain are not only useful for analyzing initial and boundary value problems found in nature, they are also useful for guiding the *design of experiments*. Hence, appreciating the existence of solutions for multiple classes of problems enables us to think more broadly when designing clever experiments to reveal new phenomena.

Appendix 4: Second Moments of Area

In Appendix 3 in Chap. 3, we defined the first moment of area and showed how it can be used to determine a centroid. Whereas

$$\iint x^1 dA, \quad \iint y^1 dA, \quad \iint z^1 dA, \tag{A4.1}$$

are called *first moments of area* (given that x, y, and z are raised to the power 1),

$$\iint x^2 dA, \quad \iint y^2 dA, \quad \iint z^2 dA, \tag{A4.2}$$

are called *second moments of area* for obvious reasons. (Note: The word "moment" is used because of the analogy of a force acting at a distance compared to the case here of an area "acting" at a distance or a distance squared. In many books, the second moments of area are called moments of inertia, but this is incorrect, for inertia must involve a mass. Moments of inertia arise in dynamics and are equally important, but different.)

Because of the quadratic form in Eq. (A4.2), additional second moments of area are possible:

$$\iint xy dA, \quad \iint yz dA, \quad \iint zx dA, \tag{A4.3}$$

and similarly for yx, zy, and xz terms. Clearly, these additional cross moments would have the same value as their paired result in Eq. (A4.3). Hence, like the Cauchy stress and linearized strain, there are nine components of the second moment of area, six of which are independent with respect to a particular coordinate system.

Herein, however, we shall typically focus on the x face and, thus, moments of area in the y-z plane. We typically denote these quantities by

$$I_{zz} = \iint y^2 dA, \; I_{yy} = \iint z^2 dA, \quad I_{yz} = -\iint yz \, dA. \tag{A4.4}$$

The minus sign in I_{yz} is introduced for convenience; we will not detail this. Rather, let us focus on I_{zz} and then I_{yy}. I_{zz} is perhaps best appreciated by calculating its value for a rectangular cross section. Referring to Fig. 4.24 and locating the centroid $(\overline{y}, \overline{z})$ at $(h/2, b/2)$, we have

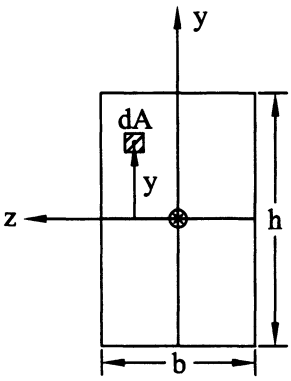

FIGURE 4.24 Schema of a rectangular cross section for purposes of determining a second moment of area.

$$I_{zz} = \int_{-b/2}^{b/2}\int_{-h/2}^{h/2}\left(y^2 dy\right)dz = \int_{-b/2}^{b/2}\left(\frac{1}{3}y^3\Big|_{-h/2}^{h/2}\right)dz$$
$$= \int_{-b/2}^{b/2}\frac{1}{3}\left(\frac{h^3}{8}+\frac{h^3}{8}\right)dz = \frac{1}{12}h^3\left(z\big|_{-b/2}^{b/2}\right) = \frac{1}{12}bh^3. \tag{A4.5}$$

A general equation for rectangular cross sections can thus be written as

$$I_{zz} = \frac{1}{12}(\text{base})(\text{height})^3, \tag{A4.6}$$

where base is the width of the cross section in the z direction and height is the length of the cross section in the vertical direction.

Next, let us consider a circular cross section (Fig. 4.25). Noting that

$$y = r\cos\theta, \quad z = r\sin\theta \tag{A4.7}$$

and

$$dA = dy\,dz = r\,d\theta dr, \tag{A4.8}$$

then

$$I_{zz} = \iint y^2 dydz = \int_0^{2\pi}\int_0^c \left(r^2\cos^2\theta\right)rdrd\theta$$
$$= \int_0^{2\pi}\left(\cos^2\theta\right)d\theta\int_0^c r^3 dr = \left(\tfrac{1}{2}\theta+\tfrac{1}{4}\sin 2\theta\right)\Big|_0^{2\pi}\left(\tfrac{1}{4}r^4\right)\Big|_0^c = \frac{\pi}{4}c^4. \tag{A4.9}$$

Here, observe two things. First, the derivation for the cylindrical cross section was easier in cylindrical coordinates, reminding us that coordinate systems

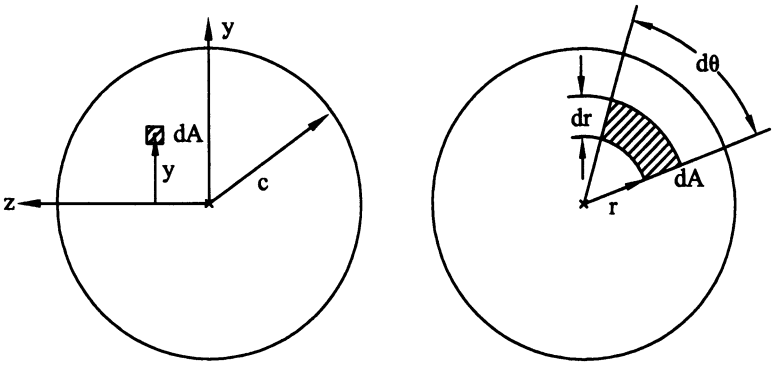

FIGURE 4.25 Schema of a circular cross section for purposes of determining a second moment of area relative to Cartesian or cylindrical coordinate systems; the latter is called the polar second moment of area and commonly denoted by J.

should be selected to facilitate analysis. Second, it is easily shown (do it) that $I_{yy} = \pi c^4/4$ also. Indeed, let us note that

$$I_{yy} + I_{zz} = \iint z^2 dA + \iint y^2 dA = \iint (z^2 + y^2) dA, \tag{A4.10}$$

where $z^2 + y^2 = r^2$ in cylindricals. Thus,

$$I_{yy} + I_{zz} = \iint r^2 r\, dr d\theta \equiv J, \tag{A4.11}$$

the so-called *polar second moment of area*. For the circular cross section, therefore,

$$J = I_{yy} + I_{zz} = 2\left(\frac{\pi}{4} c^4\right) = \frac{\pi}{2} c^4, \tag{A4.12}$$

a result that we have found to be very useful in this chapter on torsion.

Exercises

4.1 Find $\sigma_{z\theta}$, $\sigma'_{z\theta}$, and $\sigma'_{zz})_{\max}$ given a positive torque T_o applied at the free end of a constant-diameter solid shaft of radius c and length L and having a shear modulus G. Assume the shaft is fixed at the left end.

4.2 Given the shaft in the following figure, (a) find the maximum shear stress $\sigma'_{z\theta})_{\max}$ and note its location, (b) find the angle of twist Θ at the end of the shaft, and (c) find the maximum normal stress $\sigma'_{zz})_{\max}$.

FIGURE 4.26

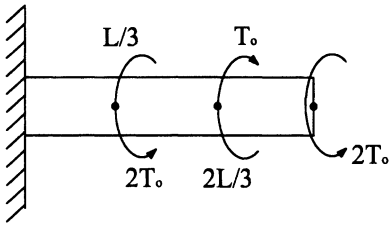

Assume a LEHI behavior, with a shear modulus G, as well as a length L and radius c (Fig. 4.26).

4.3 A laboratory test involves "potting" part of the femur in cement and then applying two loads f, each at a distance d from the centerline (cf. Fig. 4.4); this yields a couple or twisting moment $T_o = 2fd$. A strain gauge is placed at an angle α on the bone a distance $L/2$ from the fixed end. Derive a formula for the strain in the gauge that can be related to experimentally measurable quantities. Assume the bone exhibits a LEHI behavior and that it has a cross section at $z = L$ given by inner and outer radii of a and c. Discuss for what such an experiment could be utilized. Discuss why the strain gauge is not applied at length L and angle $\alpha = 0$.

4.4 For a solid shaft of diameter d for $z \in [0, 2L/3)$ and diameter nd for $z \in (2L/3, L]$, subject to torques T_o at $2L/3$ and $2T_o$ at L, (a) find the value of n such that the maximum shear stress $\sigma_{z\theta}$ is the same in each segment and (b) find the twist Θ at the free end if $n = 1$.

4.5 Some papillary muscles in the heart (which connect the valves to the endocardium through the chordae) are nearly cylindrical. We wish to perform a torsion test on such a tissue, but measuring the applied torque is difficult because of the small size. Assume that we can use the device in Fig. 4.20, that the wire is made of copper, and that the distance between points A and B is 15 mm. Also assume Θ_A and Θ_B are measurable, their difference being ~90°. If the maximum torque achieved is ~0.5 mN mm, find an appropriate diameter for the wire.

4.6 Carter and Beaupré (2001) discuss an interesting finding by Lanyon and Rubin in 1984. It was suggested that the number of cycles of loading per day and the maximum achieved strain both serve as mechanobiological stimuli for bone growth. In particular, they found that bone mass was maintained (i.e., production and removal were balanced) given a strain history of 4 cycles/day at a maximum value of 0.002 or similarly at 100 cycles/day at a maximum value between 0.0005 and 0.001 (assume 0.0008). They suggested that these combined effects can be accounted for via a "daily bone stimulus" parameter ξ that is computed via the following formula

$$\xi = \left(\sum_{\text{day}} n\varepsilon^m \right)^{1/m}$$

where n is the number of cycles/day, ε is the maximum strain attained per cycle, and m is an empirically determined material parameter. Given the data listed here, find a value for m.

4.7 Based on the results of the previous exercise, determine the number of cycles that one should walk per day if the strain during normal walking is 400 $\mu\varepsilon$ (i.e., microstrain, where $1\ \mu\varepsilon = 1 \times 10^{-6}$). Carter and Beaupré (2001) suggest that 10,000 cycles of walking per day will maintain bone mass. If the normal person advances 3 ft per stride, how far should he/she walk per day to maintain bone mass?

4.8 Based on the previous exercise and an assumed Young's modulus $E = 16$ GPa and Poisson's ratio $v = 0.325$ for bone, compute the axial load necessary to cause a strain of 400 $\mu\varepsilon$ in the normal adult diaphysial region of the femur. Express your results in terms of percent body weight, assuming a weight of 70 kg. What would the associated axial compressive stress be? Similarly, estimate the load on the femur during running and the associated compressive stress and strain. Based on these values and the previous exercise, if a person advances 4 ft per stride when running, how far should he/she run per day?

4.9 If a 17.2-Nm torque induces a maximum shearing strain of 1,132 $\mu\varepsilon$ at the periosteal surface in the diaphysial region of the femur, what is the associated value of the shearing stress if the shear modulus is 3.3 GPa?

4.10 The ratio of the cortical thickness to the outer radius of most human bones is between 0.33 and 0.4. Assume that the cross section of a segment of a long bone is circular and that the periosteal and endosteal radii are 15 mm and 9 mm, respectively. Assume, too, that a 17.2-Nm torque is applied for 10,000 cycles. What is the maximum extensional (principal) strain and, from the equation in Exercise 4.6, what is the value of the daily bone stimulus parameter ξ?

4.11 According to Carter and Beaupré (2001), "bone cross-sections that are formed are very dependent on the full history of loading throughout life. In the age range of 30–60 years, the normal bone has a diameter of about 32 mm and a cortical thickness of 5 mm. When the loads are reduced to 40 % of normal at the age of 20, the bone in later adulthood has diameter of about 30 mm and a cortical thickness of about 2 mm. The bone that forms while loads are reduced to 40 % throughout development has an adult diameter of about 22 mm and a thickness of 4 mm." What are the implications of such observations with regard to space travel, especially a voyage to Mars?

4.12 Referring to the previous exercise, note that the strains in adapting bones are generally the same regardless of the applied loads and associated cross-sectional radii. What does this suggest with regard to growth and remodeling?

4.13 Carter and Beaupré (2001, p. 81) suggest a phenomenological descriptor of bone growth (actually the rate of increase of the outer radius) of the form, $\dot{r} = \dot{r}_b + \dot{r}_m = ce^{-0.9t} + \dot{r}_m$, where $\dot{r}$ is the time rate of change of the radius, having units of microns per day; subscripts b and m denote an intrinsic biological rate and an adaptive mechanobiologic rate, respectively, and t denotes time measured in days. They suggest further that the intrinsic rate becomes relatively small shortly after birth or in early childhood, thus its representation as an exponential decay; that is, they assume that most growth and remodeling occur due to mechanobiologic factors in adolescence and maturity. In simulations, the maximum rate of biological growth was varied from 1 to 20 μm/day. Given these numbers, what would the radius be due to biological growth alone at 6 years of age? Is this value consistent with data on long bones such as the femur?

4.14 Referring to Exercise 4.13, Carter and Beaupré (2001, p. 151) note that the mass density of cancellous bone (usually ρ from 570 up to 1,200 kg/m^3) is nearly constant from early adolescence to early adulthood. They suggest that this implies that in the absence of bone diseases, the intrinsic biological rate of growth is negligible with respect to the mechanobiological rate during this period. If this is true, what are the implications with regard to the modeling of bone adapatation?

4.15 Galileo thought that long bones were hollow because this afforded maximum strength with minimum weight. Discuss this in terms of the ability of a hollow versus a solid cylindrical bone of the same mass to resist a torque; assume the bone is cortical, which has a mass density of ~1,700 kg/m^3. Alternatively, is the "hollowness" of a long bone consistent with a stress- or strain-based growth model wherein a maximum compressive strain of 1,000 $\mu\varepsilon$ is homeostatic—assume that the bone is either subjected to a torque alone or to a combined torque and axial load wherein the stresses due to torsion exceed those due to axial loading?

4.16 A long bone is subjected to a torsion test. Assume that the inner diameter is 0.375 in. and the outer diameter is 1.25 in., both for a circular cross section. If $E = 16$ GPa and $v = 0.325$, find the largest torque that can be applied prior to yield, where $\sigma_{\text{yield}} = 1.25$ ksi (i.e., a maximum normal stress).

4.17 A solid circular cylinder 10 cm long and 2 cm in outer radius behaves as a LEHI material with $G = 10$ GPa. If the twisting moment (torque) applied at the free end is 3 kNm, show that $J = 25.13 \times 10^{-8}$ m^4, $\Theta = 6.84^\circ$ at the free end, $\sigma_{z\theta}(r = c) = 238.76$ MPa, and $2\varepsilon_{z\theta}(r = c) = 0.02388$. Assume one end is fixed.

4.18 A rectangular bar $2 \times 2 \times 20$ cm in dimension is subjected to an axial force (uniform) of 4×10^6 N. Assuming $E = 100$ GPa and $v = 0.30$, find σ_{xx}, ε_{xx}, $\varepsilon_{yy} = \varepsilon_{zz}$, and the deformed dimensions (assuming homogenous strains).

4.19 A human femur is mounted in a torsion testing device and loaded to failure. Assuming that one end is fixed and the other rotated, failure (fracture) occurs when $T = 180$ Nm and $\Theta(L) = 20°$. Assume that $L = 37$ cm and that the failure occurs at 25 cm from the fixed end, where the inner and outer radii are 7 mm and 13 mm, respectively. Find the value of the shear stress at which fracture occurs; estimate the shear modulus G. Finally, note that "torsional fractures are usually initiated at regions of the bones where the cross-sections are the smallest. Some particularly weak sections of human bones are the upper and lower thirds of the humerus, femur, and fibula; the upper third of the radius; and the lower fourth of the ulna and tibia" (Özkaya and Nordin 1999).

4.20 A rectangular aluminum bar (~1.5×2.1 cm in cross section) and a circular steel rod (~1 cm in radius) are each subjected to an axial force of 20 kN. Assuming that both are 30 cm long in their unloaded configuration, find (a) the stress in each, (b) the extensional strain in each, and (c) the amount of lengthening in each. Let $E = 70$ GPa for aluminum and 200 GPa for steel.

4.21 A *brittle* behavior is characterized by an abrupt fracture soon after the elastic limit is exceeded. In contrast, a *ductile* behavior is characterized by a plastic behavior, including strain hardening, following yield. Recall Fig. 2.25. We know that yield and the subsequent plastic behavior are governed by shear stresses, which cause atoms to "slip" past one another irreversibly. Hence, it is important to compute the maximum shear stress. Although a shear stress at which a material yields is easy to determine in a torsion test, tensile tests are more common. Recall from Chap. 2, therefore, that the maximum shear stress in a 1-D tension test $\left(\sigma_{xx} = \sigma_1, \sigma_{yy} = 0, \sigma_{xy} = 0\right)$ is

$$\sigma'_{xy})_{\max} = \sqrt{\left(\frac{\sigma_1 - 0}{2}\right)^2 + 0^2} = \frac{\sigma_1}{2}.$$

This value of σ_1 at yield is called σ_y, the *yield stress*. Hence, a yield criterion in uniaxial tension is as follows: If $|\sigma_{xx}| \leq \sigma_y$, then the material has not yielded. In multiaxial states of stress, more general yield criteria are needed. Two common yield theories are the *Tresca* yield condition and the *von Mises* yield conditions. Research these two yield theories and submit a two-page summary.